

Cusps in $K \rightarrow 3\pi$ decays: a theoretical framework

Jürg Gasser^a, Bastian Kubis^b, Akaki Rusetsky^b

^aAlbert Einstein Center for Fundamental Physics, Institute for Theoretical Physics, University of Bern,
Sidlerstr. 5, CH-3012 Bern, Switzerland

^bHelmholtz-Institut für Strahlen- und Kernphysik and Bethe Center for Theoretical Physics, Universität Bonn,
Nussallee 14–16, D-53115 Bonn, Germany

Abstract

Based on the analysis of $6.031 \times 10^7 K^\pm \rightarrow \pi^0 \pi^0 \pi^\pm$ decays, the NA48/2 collaboration has recently determined the S-wave $\pi\pi$ scattering lengths $a_0 - a_2$ with high precision. In addition, the scattering length a_2 has been independently measured, although less precisely so. The present article discusses in detail one of the theoretical frameworks used in the data analysis.

Keywords: Chiral symmetries, General properties of QCD, Chiral Lagrangians, Meson–meson interactions

PACS: 11.30.Rd, 12.38.Aw, 12.39.Fe, 13.75.Lb

1. Introduction

Half a century ago, Budini and Fonda [1] investigated the threshold singularities in $K^\pm \rightarrow \pi^0 \pi^0 \pi^\pm$ decays and showed that $\pi\pi$ rescattering generates a cusp in the partial decay rate $d\Gamma/dE_{\pi^\pm}$. The strength of the cusp is determined by the amplitude for the reaction $\pi^+ \pi^- \rightarrow \pi^0 \pi^0$. Budini and Fonda provided an analytic formula for the cusp behavior and pointed out that, in principle, this decay allows one to measure the $\pi\pi$ S-wave scattering length $a_0 - a_2$, where the a_I denote the scattering lengths of definite isospin $I = 0, 2$. There were only a handful of $K \rightarrow 3\pi$ decays available in those days, and it was impossible for the authors to actually determine a_0, a_2 in this manner. The method was then forgotten and rediscovered 45 years later by Cabibbo in his seminal work [2] on the interpretation of the cusp detected in data on $K \rightarrow 3\pi$ decays, collected by the NA48/2 collaboration [3].

In the last decade, spectacular progress has been achieved concerning the knowledge of $\pi\pi$ interactions, in theory as well as in experiment. As for theory, the scattering lengths were predicted with percent level accuracy [4, 5],

$$a_0 = 0.220 \pm 0.005, \quad a_2 = -0.0444 \pm 0.0010, \quad a_0 - a_2 = 0.265 \pm 0.004, \quad (1.1)$$

within a framework which combines Roy equations [6] and chiral perturbation theory [7, 8]. On the experimental side, progress was mainly achieved through the analysis of three specific processes. First, pionium decays into two neutral pions allow one to measure $|a_0 - a_2|$ [9, 10].

Email addresses: gasser@itp.unibe.ch (Jürg Gasser), kubis@hiskp.uni-bonn.de (Bastian Kubis), rusetsky@hiskp.uni-bonn.de (Akaki Rusetsky)

Experimental results have been published by the DIRAC collaboration [11]. Second, using Watson's theorem and numerical solutions of the Roy equations [12, 13], it is possible to determine a_0 and a_2 from $K_{\ell 4}$ decays. Experiments with spectacular statistics have been carried out in this channel also in the last decade [14, 15, 16]. Last, the above mentioned cusp in $K^\pm \rightarrow \pi^0 \pi^0 \pi^\pm$ decays has been investigated through the analysis of 6.031×10^7 such events, and a high precision value for $a_0 - a_2$ is now available [17]. It confirms the chiral prediction very nicely. Indeed, combining K_{e4} decays and the result from the cusp analysis, the most recent publication by the NA48/2 collaboration quotes [16]

$$\begin{aligned} a_0 &= 0.2210 \pm 0.0047_{\text{stat}} \pm 0.0040_{\text{syst}}, \\ a_2 &= -0.0429 \pm 0.0044_{\text{stat}} \pm 0.0028_{\text{syst}}, \\ a_0 - a_2 &= 0.2639 \pm 0.0020_{\text{stat}} \pm 0.0015_{\text{syst}}. \end{aligned} \quad (1.2)$$

It seems fair to say that the precise values Eq. (1.2) could only be obtained through a combined effort of experiment and theory. Indeed, relating experimental data to the scattering lengths is a nontrivial affair [18, 19, 20], and a precise theoretical description of the cusp behavior in the amplitude for $K^\pm \rightarrow \pi^0 \pi^0 \pi^\pm$ turns out to be quite difficult.

In their most recent data analysis [17], the NA48/2 collaboration makes use of decay amplitudes constructed along two different frameworks. In the first one [2, 21], the structure of the singularity at the cusp is investigated using unitarity, analyticity, and the cluster decomposition. In addition, an approximation scheme is used, which consists in expanding the decay amplitude in powers of $\pi\pi$ scattering lengths. The latest work [21] retains effects up to order (scattering lengths)² and omits radiative corrections.

The main purpose of the present article is a detailed description of the second method [22, 23, 24]. It uses a Lagrangian framework, which automatically satisfies unitarity and analyticity constraints and allows one to include electromagnetic contributions in a standard manner [24]. In order to retain the possibility of an expansion in powers of scattering lengths, which is a very convenient concept, a non-relativistic framework is invoked that has already proven to be useful in the description of bound states [25], see Ref. [26] for a review. The formalism has recently also found applications in various, mostly cusp-related studies [27], such as $\eta \rightarrow 3\pi$ [28, 29] and $\eta' \rightarrow \eta\pi\pi$ [30] decays, as well as in near-threshold pion photo- and electroproduction on the nucleon [31, 32]. The amplitudes for $K \rightarrow 3\pi$ decays have been evaluated within other frameworks as well. We shall come back to these in Sect. 9.

The two main difficulties we were faced with to evaluate the pertinent amplitudes are the following.

- The huge statistics available require a very precise theoretical description of the decay amplitude, which allows to determine the scattering lengths from data with high precision as well. In particular, it is mandatory to include the effects of real and virtual photons [“radiative corrections”].
- The decay amplitudes can be calculated only within a certain approximation. It is therefore mandatory to set up a power counting scheme that permits to quantify the neglected effects in an algebraic manner.

As far as we can see, quantum field theory is the only method that allows to satisfy these two requirements. Independently of the method used, one is in addition faced with the problem that

the decay amplitudes for $K \rightarrow 3\pi$ are beset with leading Landau singularities [33, 34, 35, 36, 37, 38, 39].¹ This does not come as a surprise, because we are dealing with unstable particles here.

Our article is organized as follows. In Sect. 2, a covariant, non-relativistic quantum field theory framework is set up and applied in Sect. 3 to $\pi\pi$ scattering, which plays a crucial role in the analysis of final-state interactions in $K \rightarrow 3\pi$ decays. In Sect. 4 we present the Lagrangian for $K \rightarrow 3\pi$ decays and determine the tree contributions, while one-loop effects (two-loop effects) are treated in Sect. 5 (Sect. 6). In the latter section we also evaluate the pertinent two-loop integrals in the non-relativistic theory in some detail. Vertices with six-pion couplings are shown to be of no relevance at the present accuracy in Sect. 7, while we present the structure of the complete amplitude at two-loop order in Sect. 8. A comparison with other approaches to $K \rightarrow 3\pi$ decays is provided in Sect. 9, and a summary and concluding remarks are given in Sect. 10. We have relegated technical aspects of our work to various Appendices. In particular, in Appendix A we provide the complete results for the two-loop amplitude. The explicit expressions for the pertinent two-loop integrals are given in Appendix B, and their holomorphic properties are discussed in Appendix C. In order to make certain that we were not lead astray with the non-relativistic framework, we have evaluated several of the emerging two-loop graphs in standard relativistic quantum field theory as well. In particular, in Appendix D, the case of relativistic two-loop integrals with equal pion masses is considered, while loops containing different pion masses are investigated in Appendix E. Landau singularities are considered in Appendix F, and a comparison with the non-relativistic loop integrals is performed in Appendix G. Finally, we comment on the decomposition of the amplitudes in singular and non-singular parts, as used in Ref. [21], in Appendix H.

2. Covariant non-relativistic framework

In this section, we construct a non-relativistic effective field theory for the two-particle sector, which will later be used to describe pion–pion scattering. In order to simplify the discussion, here we first give a formulation for the case of a single self-interacting scalar field $\Phi(x)$ with mass M . In the following, the theory will be extended to describe three-particle decays. The main difference to the conventional non-relativistic formalism is that our approach as developed here — despite the fact that we deal with a *non-relativistic* framework — yields *explicitly invariant* two-body scattering amplitudes.² The present form turns out to be very convenient to describe three-body decays, since, in particular, the location of the singularities in the two-body subsystems (which are generally not in the rest frame) coincide with the exact relativistic values to all orders in the non-relativistic expansion. In the conventional setting, this can be achieved only perturbatively, order by order. Such a course of action is not wrong, but very cumbersome and certainly not elegant.

In a non-relativistic theory, one assumes that the momenta of all particles are much smaller than their masses. The question of the *domain of applicability* of the non-relativistic description is very subtle and depends on the dynamics of the particles considered.³ This issue will be

¹In the following, we adhere to the notation used in Refs. [37, 40] and use “*anomalous threshold*” as a synonym for “leading Landau singularity”.

²For an elementary introduction to the essentials of the conventional setting in the context of the $\pi\pi$ scattering, see, e.g., Ref. [26] and references therein.

³We remind the reader that we are designing an approach with the intention to deal with the rescattering of pions in the final state of $K \rightarrow 3\pi$ decays. However, as it is easy to check, the maximal momenta of the pions in this decay are of the order of the pion mass and thus the applicability of the non-relativistic theory in this case is not *a priori* clear.

discussed in detail in the following sections. For the moment we merely assume that using the non-relativistic framework can be justified, and proceed with its precise formulation.

Constructing an effective field theory implies setting certain counting rules. We formalize the definition of the non-relativistic domain by introducing a generic small parameter ϵ and postulating the following counting rules in this parameter.

- The mass M is to be counted as $O(1)$;
- all 3-momenta are counted as $|\mathbf{p}_i| = O(\epsilon)$;
- consequently, the kinetic energies are counted as $T_i = p_i^0 - M = O(\epsilon^2)$.

The modified approach differs from the conventional one in two aspects. First, the usual non-relativistic propagator has a pole at $p^0 = M + \mathbf{p}^2/2M$ that corresponds to the non-relativistic dispersion law. The higher-order corrections to this dispersion law are treated perturbatively, so that the results of loop calculations with the non-relativistic propagators can be made Lorentz-invariant only approximately, at a given order in the expansion in M^{-1} . In the modified framework, these higher-order corrections to the one-particle propagator are summed up, leading to the relativistic dispersion law $p^0 = w(\mathbf{p}) \doteq \sqrt{\mathbf{p}^2 + M^2}$.

The second modification is related to the matching of the non-relativistic and relativistic theories. In the conventional non-relativistic approach, the matching condition between two-body scattering amplitudes, which fixes the values of the non-relativistic couplings in terms of the parameters of the underlying relativistic theory, reads (see, e.g., Ref. [26])

$$\prod_{i=1}^4 (2w(\mathbf{p}_i))^{1/2} T_{NR}(\mathbf{p}_3, \mathbf{p}_4; \mathbf{p}_1, \mathbf{p}_2) = T_R(\mathbf{p}_3, \mathbf{p}_4; \mathbf{p}_1, \mathbf{p}_2), \quad (2.1)$$

where the subscripts NR (R) stand for the non-relativistic (relativistic) amplitudes. The additional factors $(2w(\mathbf{p}_i))^{1/2}$ for each external leg account for the different normalization of the non-relativistic and relativistic states.

Since Eq. (2.1) is not explicitly covariant, the matching condition is different in different reference frames. For simplicity, we consider matching at threshold, where the relativistic amplitude is merely a constant $T_R(\mathbf{p}_3, \mathbf{p}_4; \mathbf{p}_1, \mathbf{p}_2)|_{\text{thr}} = A$ in all reference frames. On the other hand, the non-relativistic amplitude at threshold in different frames, obtained by expanding Eq. (2.1) in momenta, is given by

$$T_{NR}(\mathbf{p}_3, \mathbf{p}_4; \mathbf{p}_1, \mathbf{p}_2)|_{\text{thr}} = \frac{A}{4M^2} - \frac{A}{16M^4} \mathbf{P}^2 + \dots, \quad (2.2)$$

where \mathbf{P} denotes the total 3-momentum of the particles 1 and 2 at threshold. Let us now limit ourselves to the tree approximation and suppose that one wishes to write down the non-relativistic effective Lagrangian that reproduces Eq. (2.2) in this approximation. Such a Lagrangian would have to consist of an infinite tower of operators, whose couplings are determined by a single constant A . This again means that Lorentz invariance can be taken into account only perturbatively, order by order in the expansion in M^{-1} . Once more this procedure, albeit formally correct, looks rather awkward and renders higher-order calculations cumbersome.

In the particular case considered above, it is clear that the problem disappears if we arrange the non-relativistic theory in a way such that the overall non-invariant factor on the left-hand side of Eq. (2.1) disappears. This can be achieved by a non-local rescaling of the non-relativistic

field $\Phi(x) \rightarrow \sqrt{2W} \Phi(x)$, where $W = \sqrt{M^2 - \Delta}$. In the modified theory, the normalization of the 1-particle states is given by the relativistic expression $\langle \mathbf{p} | \mathbf{q} \rangle = 2w(\mathbf{p})(2\pi)^3 \delta^3(\mathbf{p} - \mathbf{q})$, whereas the matrix element of the free field operator between the vacuum and the one-particle state is normalized to unity: $\langle 0 | \Phi(0) | \mathbf{p} \rangle = 1$. The Lagrangian with the rescaled field is given by

$$\mathcal{L} = \Phi^\dagger 2W(i\partial_t - W)\Phi + C(\Phi^\dagger)^2 \Phi^2 + \dots, \quad (2.3)$$

where C denotes the lowest-order ($\mathcal{O}(1)$) four-particle coupling and the ellipsis stands for four-point interactions with derivatives (these terms count as $\mathcal{O}(\epsilon^2)$ and higher). Note that the above Lagrangian is non-local since it contains square roots of a differential operator. Heavy-particle number should be conserved in the non-relativistic theory by construction (see, e.g., Ref. [26]). The matching condition in tree approximation yields $T_{NR} = 4C = A$ in all reference frames or, in other words, the truncation of the higher-derivative terms in the Lagrangian does not render the non-relativistic amplitude non-invariant.

The propagator in the rescaled theory is given by

$$i\langle 0 | T \Phi(x) \Phi^\dagger(y) | 0 \rangle = \int \frac{d^4 p}{(2\pi)^4} \frac{e^{-ip(x-y)}}{2w(\mathbf{p})(w(\mathbf{p}) - p_0 - i\epsilon)}. \quad (2.4)$$

From now on, we shall not display $i\epsilon$ in the propagators explicitly. Our next goal will be to demonstrate that

- in the above effective theory, the counting rules in ϵ , established at tree level, are not destroyed by loop corrections;
- the amplitude is explicitly Lorentz-invariant also in the presence of loops.

Since all loop diagrams in the non-relativistic approach to the two-particle sector can be expressed through the elementary bubble integral

$$J(P^0, \mathbf{P}) = \int \frac{d^D l}{(2\pi)^D} \frac{1}{2w(\mathbf{l})2w(\mathbf{P} - \mathbf{l})(w(\mathbf{l}) - l^0)(w(\mathbf{P} - \mathbf{l}) - P^0 + l^0)}, \quad (2.5)$$

we concentrate on this integral below. The quantity $J(P^0, \mathbf{P})$ is calculated in an arbitrary reference frame characterized by the total 4-momentum $P = (P^0, \mathbf{P})$. Calculations are done in dimensional regularization, D is the number of space-time dimensions and $d = D - 1$.

To begin with, we note that naïve power counting predicts $J(P^0, \mathbf{P})$ to be of $\mathcal{O}(\epsilon^{d-2})$: each propagator in the integral scales as $\mathcal{O}(\epsilon^{-2})$, while the integration measure, with d momenta and one energy integration, contributes a power ϵ^{d+2} . It can be checked by straightforward calculation that the loop given by Eq. (2.5) violates this power counting prediction. This is a well-known phenomenon, caused by the presence of the heavy mass scale M in the integrand. In order to circumvent this problem, usual Feynman rules in the effective theory have to be supplemented by some additional prescription that annihilates the high-energy contribution (coming from the integration momenta of order M) to the Feynman integral. We choose a particular prescription referred to as the “threshold expansion” [41] (see also Refs. [26, 42] for a focused discussion of the issue within non-relativistic effective theories). The prescription defines how the square roots present in the particle propagators are handled in the calculations. According to the prescription, one expands the integrand in a Feynman integral in inverse powers of the heavy scale M , integrates the resulting series term by term in dimensional regularization, and finally sums up the results.

Let us see how this prescription can be realized in practice. We perform the integration over l^0 in Eq. (2.5) by using Cauchy's theorem and rewrite $J(P^0, \mathbf{P})$ as

$$J(P^0, \mathbf{P}) = \int \frac{d^d l}{(2\pi)^d} \frac{1}{4w(\mathbf{l})w(\mathbf{P}-\mathbf{l})} \frac{1}{w(\mathbf{l})+w(\mathbf{P}-\mathbf{l})-P^0}. \quad (2.6)$$

Further, performing the shift $\mathbf{l} \rightarrow \mathbf{l} + \mathbf{P}/2$, we transform the integrand by using the identity

$$\begin{aligned} & \frac{1}{4w_a w_b} \left\{ -\frac{1}{P^0 - w_a - w_b} - \frac{1}{P^0 + w_a + w_b} + \frac{1}{P^0 + w_a - w_b} + \frac{1}{P^0 - w_a + w_b} \right\} \\ &= \frac{1}{2P^0} \frac{1}{\mathbf{l}^2 - (\mathbf{P}/P^0)^2 - q_0^2}, \end{aligned} \quad (2.7)$$

where $w_a = w(\mathbf{P}/2 + \mathbf{l})$, $w_b = w(\mathbf{P}/2 - \mathbf{l})$, $q_0^2 = s/4 - M^2$, and $s \doteq P^2 = (P^0)^2 - \mathbf{P}^2$.

Next, we investigate how the threshold expansion affects the result of the integration. According to power counting, $w_a - M$, $w_b - M = O(\epsilon^2)$ and $P^0 - 2M = O(\epsilon^2)$. Consequently, expanding the last three terms in Eq. (2.7) in powers of ϵ generates polynomials in the integration momentum \mathbf{l} . Recalling that integrals containing only powers of \mathbf{l} vanish in dimensional regularization, we finally conclude that using the threshold expansion enables us to rewrite the integral in Eq. (2.6) as

$$J(P^0, \mathbf{P}) = \int \frac{d^d l}{(2\pi)^d} \frac{1}{2P^0} \frac{1}{\mathbf{l}^2 - (\mathbf{P}/P^0)^2 - q_0^2}. \quad (2.8)$$

It is seen that the heavy scale M has disappeared as a result of the threshold expansion.

In order to perform the integral in Eq. (2.8), we choose the first axis along the momentum \mathbf{P} , so that $\mathbf{P} = (|\mathbf{P}|, \mathbf{0})$ and $\mathbf{l} = (l_1, \mathbf{l}_\perp)$. Rescaling $l_1 \rightarrow l_1 P^0 / \sqrt{s}$ and doing the momentum integration, we finally arrive at

$$J(P^0, \mathbf{P}) \doteq J(s) = \frac{i}{16\pi} \left(1 - \frac{4M^2}{s}\right)^{1/2} + O(d-3). \quad (2.9)$$

Note also that $J(s)$ coincides with the imaginary part of the relativistic one-loop integral.

The non-relativistic amplitude in the absence of derivative couplings is given by the bubble sum

$$T_{NR}(\mathbf{p}_3, \mathbf{p}_4; \mathbf{p}_1, \mathbf{p}_2) = 4C + 8C^2 J(s) + 16C^3 J(s)^2 + \dots \quad (2.10)$$

The inclusion of derivative couplings is straightforward. We restrict ourselves to order ϵ^2 , where the real part of the relativistic scattering amplitude of two identical particles can be parameterized in terms of two constants A and B , which are related to the S-wave scattering length and the effective range,

$$\begin{aligned} \text{Re } T_R(\mathbf{p}_3, \mathbf{p}_4; \mathbf{p}_1, \mathbf{p}_2) &= A + B(s - 4M^2) + O(\epsilon^4) \\ &= A + B(p_1 p_2 + p_3 p_4 - 2M^2) + O(\epsilon^4). \end{aligned} \quad (2.11)$$

The term with two derivatives in the non-relativistic effective Lagrangian can be directly read off from Eq. (2.11), leading to

$$\mathcal{L}^{(2)} = D \left\{ (W\Phi^\dagger W\Phi^\dagger \Phi^2 + \nabla\Phi^\dagger \nabla\Phi^\dagger \Phi^2 - M^2(\Phi^\dagger)^2 \Phi^2) + h.c. \right\}, \quad (2.12)$$

with $4D = B + C^3/(64\pi^2 M^2)$. Again, this Lagrangian is non-local, and the factor W should be expanded in actual calculations.

We summarize our main findings up to this point.

1. If the threshold expansion is applied, the one-loop integral $J(s)$ counts as $\mathcal{O}(\epsilon)$, so the loops do not violate power counting.
2. The insertion of derivative couplings does not violate power counting.
3. $J(s)$ is explicitly Lorentz-invariant. Since the tree-level amplitude is also invariant, so is the scattering amplitude at any given order in the perturbative expansion. This statement is trivial for non-derivative couplings only; one can easily ensure that it still holds in the presence of derivative couplings in the scattering amplitude.
4. According to Eq. (2.9), $J(s = 4M^2) = 0$. This means in particular that the coupling constant C is proportional to the scattering length *to all orders in perturbation theory*. In general, the coupling constants of the non-relativistic theory are expressed through the effective-range expansion parameters in the two-particle sector. If in the following this non-relativistic Lagrangian is used to evaluate pion–pion rescattering effects in the three-particle decay in perturbation theory, the result will be written in terms of these parameters. This property constitutes the major advantage of the non-relativistic approach as compared to a relativistic framework. For example, the decay amplitude calculated in chiral perturbation theory is given as an expansion in the quark masses, not in the scattering lengths; if one attempts to extract the values of the scattering lengths from the data on three-particle decays, the accuracy of the former representation may not suffice.

The generalization of this method to higher orders and to the case of non-identical particles with different masses can be performed in a straightforward manner.

We conclude this section by a remark about the terminology used. We still refer to the above framework as “non-relativistic,” albeit the energies and momenta of particles in this approach obey relativistic dispersion laws. In our naming scheme, “non-relativistic theory” denotes a theory in which *explicit antiparticle degrees of freedom* are absent (respectively, are included in the couplings of the effective Lagrangian), and the number of particles is preserved in each interaction vertex.

3. Non-relativistic approach to $\pi\pi$ scattering

3.1. Lagrangian and scattering amplitude

Now we apply the modified non-relativistic framework to the $\pi\pi$ scattering amplitudes. The masses of charged and neutral pions $M_{\pi^\pm} \doteq M_\pi$ and M_{π^0} are taken to be different, but virtual photons are not included at this stage. Due to the inelastic coupling of the $\pi^+\pi^-$ and the $\pi^0\pi^0$ channels, a consistent power counting requires the quantity $\Delta_\pi = M_\pi^2 - M_{\pi^0}^2$ to be counted as $\mathcal{O}(\epsilon^2)$. We consider the following five physical channels in $\pi^a\pi^b \rightarrow \pi^c\pi^d$: $(ab; cd) = (1) (00; 00)$, $(2) (+0; +0)$, $(3) (+-; 00)$, $(4) (+-; +-)$, $(5) (++; ++)$. The Lagrangian takes the form

$$\mathcal{L}_{\pi\pi} = \sum_{\pm} \Phi_{\pm}^{\dagger} 2W_{\pm} (i\partial_t - W_{\pm}) \Phi_{\pm} + \Phi_0^{\dagger} 2W_0 (i\partial_t - W_0) \Phi_0 + \sum_{i=1}^5 \mathcal{L}_i, \quad (3.1)$$

where Φ_i is the non-relativistic pion field operator and $W_{\pm} = \sqrt{M_{\pi}^2 - \Delta}$, $W_0 = \sqrt{M_{\pi^0}^2 - \Delta}$, with Δ the Laplacian. We furthermore introduce the notation

$$\begin{aligned} (\Phi_n)_{\mu} &= (\mathcal{P}_n)_{\mu} \Phi_n, & (\Phi_n)_{\mu\nu} &= (\mathcal{P}_n)_{\mu} (\mathcal{P}_n)_{\nu} \Phi_n, & (\mathcal{P}_n)_{\mu} &= (W_n, -i\nabla), \\ (\Phi_n^{\dagger})_{\mu} &= (\mathcal{P}_n^{\dagger})_{\mu} \Phi_n^{\dagger}, & (\Phi_n^{\dagger})_{\mu\nu} &= (\mathcal{P}_n^{\dagger})_{\mu} (\mathcal{P}_n^{\dagger})_{\nu} \Phi_n^{\dagger}, & (\mathcal{P}_n^{\dagger})_{\mu} &= (W_n, i\nabla), \end{aligned} \quad (3.2)$$

for $n = a, b, c, d$, in order to write the interaction Lagrangian in the form

$$\begin{aligned} \mathcal{L}_i &= x_i C_i (\Phi_c^{\dagger} \Phi_d^{\dagger} \Phi_a \Phi_b + h.c.) \\ &+ x_i D_i \{ (\Phi_c^{\dagger})_{\mu} (\Phi_d^{\dagger})^{\mu} \Phi_a \Phi_b + \Phi_c^{\dagger} \Phi_d^{\dagger} (\Phi_a)_{\mu} (\Phi_b)^{\mu} - h_i \Phi_c^{\dagger} \Phi_d^{\dagger} \Phi_a \Phi_b + h.c. \} \\ &+ \frac{u_i E_i}{2} \{ [(\Phi_c^{\dagger}) (\Phi_d^{\dagger})^{\mu} - (\Phi_c^{\dagger})^{\mu} \Phi_d^{\dagger}] [(\Phi_a)_{\mu} \Phi_b - \Phi_a (\Phi_b)_{\mu}] + h.c. \} + \dots, \end{aligned} \quad (3.3)$$

with $h_i = \bar{s}_i - \frac{1}{2} (M_a^2 + M_b^2 + M_c^2 + M_d^2)$, where \bar{s}_i denotes the physical threshold in the i th channel. Explicitly, $h_1 = 2M_{\pi^0}^2$, $h_2 = 2M_{\pi} M_{\pi^0}$, $h_3 = 3M_{\pi}^2 - M_{\pi^0}^2$, $h_4 = h_5 = 2M_{\pi}^2$. The ellipsis stands for terms of order ϵ^4 . The low-energy constants C_i , D_i , E_i are matched to the physical scattering lengths below. To simplify the resulting expressions, we have furthermore introduced the scaling $x_1 = x_5 = 1/4$, $x_2 = x_3 = x_4 = 1$, $u_1 = u_3 = u_5 = 0$, $u_2 = u_4 = 1$. Finally, note that we do not discuss local six-pion couplings here, which can potentially play a role in the rescattering of three-pion final states; we will comment on these in some detail in Sect. 7.

Evaluating the non-relativistic scattering amplitude up to order ϵ^2 with the use of the above Lagrangian, we obtain

$$\begin{aligned} T_{NR}^{00} &= 2C_{00} + 2D_{00}(s - \bar{s}_{00}) + 2C_{00}^2 J_{00}(s) + 4C_x^2 J_{+-}(s) \\ &+ 2C_{00}^3 (J_{00}(s))^2 + 8C_{00} C_x^2 J_{00}(s) J_{+-}(s) + 8C_x^2 C_{+-} (J_{+-}(s))^2 + \dots, \\ T_{NR}^{+0} &= 2C_{+0} + 2D_{+0}(s - \bar{s}_{+0}) + E_{+0}(t - u) + 4C_{+0}^2 J_{+0}(s) + 8C_{+0}^3 (J_{+0}(s))^2 + \dots, \\ T_{NR}^x &= 2C_x + 2D_x(s - \bar{s}_x) + 4C_x C_{+-} J_{+-}(s) + 2C_x C_{00} J_{00}(s) + 8C_{+-}^2 C_x (J_{+-}(s))^2 \\ &+ 4(C_{+-} C_x C_{00} + C_x^3) J_{+-}(s) J_{00}(s) + 2C_{00}^2 C_x (J_{00}(s))^2 + \dots, \\ T_{NR}^{+-} &= 2C_{+-} + 2D_{+-}(s - \bar{s}_{+-}) + E_{+-}(t - u) + 4C_{+-}^2 J_{+-}(s) + 2C_x^2 J_{00}(s) \\ &+ 8C_{+-}^3 (J_{+-}(s))^2 + 8C_{+-} C_x^2 J_{+-}(s) J_{00}(s) + 2C_x^2 C_{00} (J_{00}(s))^2 + \dots, \\ T_{NR}^{++} &= 2C_{++} + 2D_{++}(s - \bar{s}_{++}) + 2C_{++}^2 J_{++}(s) + 2C_{++}^3 (J_{++}(s))^2 + \dots, \end{aligned} \quad (3.4)$$

where \bar{s}_i denotes the threshold in the pertinent channel $\bar{s}_{00} = 4M_{\pi^0}^2$, $\bar{s}_{+0} = (M_{\pi} + M_{\pi^0})^2$, $\bar{s}_x = \bar{s}_{+-} = \bar{s}_{++} = 4M_{\pi}^2$. Further, in order to make the expressions more transparent, we have modified the notation according to

$$\{C_1, C_2, C_3, C_4, C_5\} \rightarrow \{C_{00}, C_{+0}, C_x, C_{+-}, C_{++}\}, \quad (3.5)$$

and similarly for D_i and E_i . Finally, $J_{ab}(s)$ denotes the generalization of the loop function $J(s)$ given by Eqs. (2.5) and (2.9) to the case of unequal masses M_a and M_b , which is obtained from Eq. (2.5) by replacing $w(\mathbf{l}) \rightarrow w_a(\mathbf{l})$, $w(\mathbf{P} - \mathbf{l}) \rightarrow w_b(\mathbf{P} - \mathbf{l})$ and $w_{a,b}(\mathbf{k}) = (M_{a,b}^2 + \mathbf{k}^2)^{1/2}$. This function is equal to

$$J_{ab}(s) = \frac{i}{16\pi} v_{ab}(s), \quad v_{ab}^2(s) = \frac{4q_{ab}^2(s)}{s} = \frac{\lambda(s, M_a^2, M_b^2)}{s^2}, \quad (3.6)$$

with the usual Källén function $\lambda(a, b, c) = a^2 + b^2 + c^2 - 2(ab + ac + bc)$.

For the purely elastic channels (+0) and (++) , Eq. (3.4) can be directly compared to the effective-range expansion of the relativistic $\pi\pi$ scattering amplitudes

$$T_R^i = 32\pi \sum_{l=0}^{\infty} (2l+1) t_l^i P_l(z), \quad i = +0, ++$$

$$\text{Re } t_0^i = A_i + B_i q_i^2 + \mathcal{O}(\epsilon^4), \quad \text{Re } t_1^i = q_i^2 A_i^P + \mathcal{O}(\epsilon^4), \quad (3.7)$$

where the t_l^i are the partial waves of the respective (physical) channel i , A_i , B_i , A_i^P the corresponding S-wave scattering length and effective range as well as the P-wave scattering length, and $z = \cos\theta$ is the cosine of the center-of-mass scattering angle. In the isospin symmetric limit at $M_\pi = 139.6$ MeV, which we denote by \bar{C}_i etc., the matching relations are of the form

$$2\bar{C}_{+0} = \bar{C}_{++} = 16\pi a_2, \quad 2\left(\bar{D}_{+0} - \frac{\bar{C}_{+0}^3}{(32\pi M_\pi)^2}\right) = \bar{D}_{++} - \frac{\bar{C}_{++}^3}{(32\pi M_\pi)^2} = 4\pi b_2, \quad \bar{E}_{+0} = 12\pi a_1, \quad (3.8)$$

with the $I = 1$ P-wave scattering length $a_1 = (0.379 \pm 0.005) \times 10^{-1} M_\pi^{-2}$ in addition to the S-wave scattering lengths of definite isospin $I = 0, 2$ quoted in Eq. (1.1) [4, 5]. For the remaining channels, the situation is more complicated due to the coupling of the $\pi^+\pi^-$ and $\pi^0\pi^0$ channels with their different thresholds. In the isospin limit, with both thresholds coinciding, one has matching relations also for these similar to Eq. (3.8), and the coefficients \bar{C}_i and \bar{E}_i are related to the $\pi\pi$ scattering lengths according to

$$\bar{C}_{00} = \frac{16\pi}{3}(a_0 + 2a_2), \quad \bar{C}_x = \frac{16\pi}{3}(a_2 - a_0), \quad \bar{C}_{+-} = \frac{8\pi}{3}(2a_0 + a_2), \quad \bar{E}_{+-} = 12\pi a_1. \quad (3.9)$$

The relations for the \bar{D}_i are similar to those displayed in Eq. (3.8). However, taking the pion masses to be different, the threshold behavior for $\pi\pi$ channels of total charge zero is rather of the form (cf. Ref. [19])

$$32\pi t_0^i = \alpha^i + i\nu_+ \beta^i + i\nu_{00} \gamma^i + \nu_{+-} \nu_{00} \delta^i \quad (3.10)$$

(for the case of an S-wave), where $\alpha^i, \dots, \delta^i$ are real and analytic functions in the low-energy region on the real axis, $0 < s < 16M_{\pi^0}^2$. The above parameterization is an analog of the effective-range expansion for the $\pi\pi$ amplitudes in the presence of multiple thresholds. Although we do not make use of these expressions in the following, for illustration we show the corresponding functions for the (00) channel, up to the order displayed in Eq. (3.4), i.e. $\mathcal{O}(a^3 \epsilon^2)$, which read

$$\alpha^{00} = 2\left(C_{00} + 4D_{00}q_{00}^2 - \frac{1}{(16\pi)^2}(C_{00}^3\nu_{00}^2 + 4C_{+-}C_x^2\nu_{+-}^2)\right),$$

$$\beta^{00} = \frac{1}{4\pi}C_x^2, \quad \gamma^{00} = \frac{1}{8\pi}C_{00}^2, \quad \delta^{00} = -\frac{1}{32\pi^2}C_{00}C_x^2. \quad (3.11)$$

We note in passing that recovering the isospin limit from these coefficients is a delicate procedure: it is obvious that the second term in the q^2 -expansion of α^{00} will not coincide with the effective range in the isospin limit (up to normalization) due to the presence of the term δ^{00} . The $\beta^i, \gamma^i, \delta^i$ are not independent, though, but also these can be expressed in terms of the parameters of the effective range expansion. The constraints that enable us to determine these parameters can also be derived from (multi-channel) unitarity, which must be obeyed by the $\pi\pi$ scattering amplitudes.

The effective field-theoretical approach that we use automatically incorporates unitarity order by order.

In order to take isospin breaking in the leading $\pi\pi$ effective range parameters into account, we consider the effective $\mathcal{O}(p^2)$ Lagrangian of chiral perturbation theory

$$\mathcal{L}_{\text{eff}} = \frac{F^2}{4} \langle \partial_\mu U \partial^\mu U^\dagger + \chi U^\dagger + \chi^\dagger U \rangle + e^2 C \langle QUQU^\dagger \rangle, \quad (3.12)$$

with $\chi = 2B \text{diag}(m_u, m_d)$, $Q = \text{diag}(2, -1)/3$, and U being the standard 2×2 unitary matrix of the pion field. Further, at this order,

$$M_{\pi^0}^2 = M^2 = B(m_u + m_d), \quad M_\pi^2 = M^2 + \frac{2e^2 C}{F^2}. \quad (3.13)$$

Note that evaluating isospin breaking only at $\mathcal{O}(p^2)$ is consistent with neglecting virtual photons in the non-relativistic framework. In order to carry out the matching of the relativistic and non-relativistic theories at higher orders, it is necessary to include photons. At leading order in chiral perturbation theory one finds [43]

$$C_{00,+0,++} = \bar{C}_{00,+0,++}(1 - \eta), \quad C_x = \bar{C}_x(1 + \eta/3), \quad C_{+-} = \bar{C}_{+-}(1 + \eta), \quad (3.14)$$

where $\eta = \Delta_\pi/M_\pi^2 = 6.5 \times 10^{-2}$. Equation (3.14) shows that the threshold amplitudes, which occur in the scattering length expansion, are affected by substantial isospin breaking corrections. Isospin-breaking corrections in the effective ranges and P-wave scattering lengths (or, more precisely, in the non-relativistic couplings D_i and E_i) do not contribute at the accuracy considered here. They have been investigated in Ref. [29] and were found to be tiny.

Generalizations to higher loop orders in $\pi\pi$ scattering are straightforward. However, they are irrelevant for the calculation of $K \rightarrow 3\pi$ decays to two loops, as performed below; in fact, the corrections of $\mathcal{O}(\bar{C}_i^3)$ in the matching relations for the effective ranges Eq. (3.8) are already beyond the order needed for our purposes, as they constitute $\mathcal{O}(a^3)$ effects and only enter $K \rightarrow 3\pi$ at three loops.

3.2. Convergence of the non-relativistic expansion

We wish to briefly discuss the convergence of the non-relativistic representation of the $\pi\pi$ amplitude as given in Eq. (3.4). As an example, we show real and imaginary part of the $I = 0$ S-wave amplitude in Fig. 1 over the kinematic range accessible in $K \rightarrow 3\pi$ decays, i.e. for $4M_\pi^2 \leq s \leq (M_K - M_\pi)^2$. We compare to the Roy equation solution [12] matched to chiral perturbation theory [4, 5]. We observe that at such low energies, already the tree amplitude in Eq. (3.4), consisting merely of scattering length and effective range term, gives a very good description of the real part, see Fig. 1 (left); including the two-loop corrections hardly changes the amplitude at all. This is easily understood by simplifying the $I = 0$ S-wave two-loop amplitude with the matching relations analogous to Eq. (3.8) according to

$$\text{Re } t_0^0 = a_0 + b_0 q^2 + \frac{(a_0)^3 q^4}{M_\pi^2(M_\pi^2 + q^2)}, \quad (3.15)$$

so it differs from the tree amplitude only by terms of $\mathcal{O}(a^3 q^4)$ and higher. A further improvement requires the introduction of a shape parameter $\propto c_0 q^4$. On the other hand, the description of the

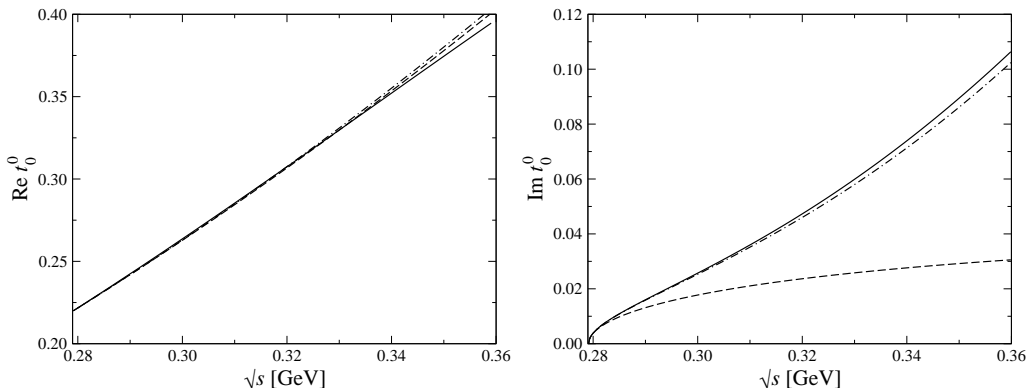


Figure 1: Convergence of the $\ell = 0$, $I = 0$ $\pi\pi$ partial wave in the non-relativistic expansion; the left panel shows the real, the right panel the imaginary part. In both cases, the full lines represent the Roy equation solution [12] matched to chiral perturbation theory [4, 5]. In the left panel, the dashed line is the non-relativistic tree-level amplitude, while the dash-dotted curve represents the two-loop representation. In the right panel, the dashed curve is the one-loop amplitude according to Eq. (3.4), while the dash-dotted is the improved one-loop representation, see main text.

imaginary part, given purely by the one-loop contributions in Eq. (3.4), misses the phenomenological amplitude completely, see Fig. 1 (right). This is also easy to explain: even in the sense of (only) perturbative unitarity, the imaginary part of $\mathcal{O}(a^2\epsilon)$ corresponds to a real part in the scattering length approximation. We have to improve the imaginary part to $\mathcal{O}(a^2\epsilon^3)$ and partial $\mathcal{O}(a^2\epsilon^5)$ by the replacement $C_i \rightarrow C_i + D_i(s - \bar{s}_i)$ in the one-loop contributions of Eq. (3.4); this improved one-loop representation is then a very good approximation to the true imaginary part at the energies relevant for $K \rightarrow 3\pi$, see also Fig. 1 (right)

Finally, we wish to anticipate the use of the $\pi\pi$ amplitudes discussed above in the cusp analysis of $K \rightarrow 3\pi$. The decay rates will be expressed in terms of the couplings C_i , D_i , E_i , \dots that are related to the physical $\pi\pi$ scattering amplitudes. Once these quantities have been determined from data (in practice, one may decide to use some of the parameters, for instance effective ranges or P-waves, as input, employing their theoretically predicted values), they can be related to the S-wave scattering lengths using the corrections displayed in Eq. (3.14). With radiative corrections applied [24], these relations must be adapted accordingly.

4. Non-relativistic approach to $K^+ \rightarrow 3\pi$ decays

4.1. Kinematics

In this and in the following sections, we develop in detail a non-relativistic framework for $K \rightarrow 3\pi$ decays by means of the particular channels $K^+(P_K) \rightarrow \pi^0(p_1)\pi^0(p_2)\pi^+(p_3)$ and $K^+(P_K) \rightarrow \pi^+(p_1)\pi^+(p_2)\pi^-(p_3)$. The method can straightforwardly be extended to neutral kaon decays – for early applications of the method, see Refs. [22, 23, 24].

The kinematical variables are defined as follows,

$$s_i \doteq (P_K - p_i)^2, \quad M_i^2 \doteq p_i^2, \\ 3s_0^0 \doteq M_K^2 + M_\pi^2 + 2M_{\pi^0}^2, \quad 3s_0^+ \doteq M_K^2 + 3M_\pi^2, \quad T_i \doteq p_i^0 - M_i, \quad i = 1, 2, 3, \quad (4.1)$$

with

$$s_1 + s_2 + s_3 = M_K^2 + \sum_i M_i^2. \quad (4.2)$$

Further, assuming that i, j, k are all different, we set

$$\Delta_i^2 \doteq \frac{\lambda(M_K^2, M_i^2, (M_j + M_k)^2)}{4M_K^2}, \quad \mathbf{Q}_i \doteq \mathbf{p}_j + \mathbf{p}_k, \quad Q_i^0 \doteq p_j^0 + p_k^0. \quad (4.3)$$

In the center-of-mass frame $P_K = (M_K, \mathbf{0})$,

$$p_i^0 = \frac{M_K^2 + M_i^2 - s_i}{2M_K}, \quad \mathbf{p}_i^2 = \frac{\lambda(M_K^2, M_i^2, s_i)}{4M_K^2}. \quad (4.4)$$

As usual, the label $i = 3$ is always assigned to the ‘‘odd’’ particle, i.e. to the π^+ in the neutral mode $K^+ \rightarrow \pi^0 \pi^0 \pi^+$ and to the π^- in the charged mode $K^+ \rightarrow \pi^+ \pi^+ \pi^-$. Note that the values of the masses M_i are channel dependent.

4.2. Lagrangian and tree amplitude

A non-relativistic approach to describe decays $K \rightarrow 3\pi$ can be justified if the typical kinetic energies T_i of the decay products are much smaller than the masses. This can be achieved by considering a world where the strange quark mass is taken to be smaller than its actual value. Then, a consistent counting scheme arises if one introduces a formal parameter ϵ (the same as in the two-particle case) and counts T_i as a term of order ϵ^2 , the pion momenta as order ϵ , whereas the pion and kaon masses are counted as $O(1)$. From $\sum_i T_i = M_K - \sum_i M_i$, one concludes that the difference $M_K - \sum_i M_i$ is then a quantity of order ϵ^2 as well. In addition, as mentioned in the previous section, the pion mass difference Δ_π must also be counted as $O(\epsilon^2)$. The effective field theory framework, which we construct below, enables us to obtain a systematic expansion of the amplitudes in ϵ . For sufficiently small m_s , the expansion in ϵ is expected to work very well.

Together with ϵ , our theory has another expansion parameter, namely a characteristic size of the $\pi\pi$ threshold parameters, which we denote generically by a . In particular, the amplitudes in the non-relativistic framework are given in form of an expansion in several low-energy couplings C_i, D_i, E_i , which can be expressed in terms of the threshold parameters of the relativistic $\pi\pi$ scattering amplitude. We expect the expansion in a to converge rapidly because of the smallness of the scattering lengths. These two expansions are correlated: because one-loop integrals are of order ϵ , adding a pion loop generated by a four-pion vertex increases both the order in a and in ϵ by one. A consistent power counting is achieved: to a given order in a and in ϵ , a well-defined finite number of diagrams contributes.

Increasing m_s to its physical value again, convergence in the ϵ -expansion is not *a priori* evident, because T_i/M_i can become as large as 0.4, and the corresponding maximal momentum $|\mathbf{p}_i|$ is then not much smaller than the pion mass. However, let us note that the non-relativistic framework is only used to correctly reproduce the non-analytic behavior of the decay amplitudes in the kinematical variables s_1, s_2, s_3 , and to thus provide a parameterization consistent with unitarity and analyticity – a trivial polynomial part in the amplitudes can be removed by a redefinition of the couplings in the Lagrangian. In addition, from the analysis of the experimental data one knows [21] that in the whole physical region the real part of the decay amplitude can be well approximated by a polynomial in s_1, s_2, s_3 with a maximum degree 2. We interpret this fact as an experimental indication for a good convergence of the ϵ -expansion for the quantities we are

interested in. In the following, when we also study the behavior of the decay amplitude in the complex energy plane away from the real axis, we therefore understand the low-energy region (or, equivalently, the non-relativistic region) to be determined as a strip enclosing the real axis from $s_i = (M_j + M_k)^2$ to $s_i = (M_K - M_i)^2$, and going slightly beyond the boundaries. The width of the strip should be smaller than the hard scale set by the pion mass squared.

We now proceed with the construction of the Lagrangian framework. Aside from the Lagrangian $\mathcal{L}_{\pi\pi}$ displayed in Eq. (3.1) that describes $\pi\pi$ final state interactions, we need the Lagrangian \mathcal{L}_K which generates genuine $K \rightarrow 3\pi$ decays, such that the complete Lagrangian is

$$\mathcal{L} = \mathcal{L}_K + \mathcal{L}_{\pi\pi}. \quad (4.5)$$

At order (scattering lengths)², the amplitudes are given by

$$\begin{aligned} \mathcal{M}_{00+} &= \mathcal{M}_N^{\text{tree}} + \mathcal{M}_N^{1\text{-loop}} + \mathcal{M}_N^{2\text{-loops}} & [K^+ \rightarrow \pi^0 \pi^0 \pi^+], \\ \mathcal{M}_{+ +-} &= \underbrace{\mathcal{M}_C^{\text{tree}}}_{\mathcal{L}_K} + \underbrace{\mathcal{M}_C^{1\text{-loop}}}_{\mathcal{L}_K \times \mathcal{L}_{\pi\pi}} + \underbrace{\mathcal{M}_C^{2\text{-loops}}}_{\mathcal{L}_K \times \mathcal{L}_{\pi\pi} \times \mathcal{L}_{\pi\pi}} & [K^+ \rightarrow \pi^+ \pi^+ \pi^-], \end{aligned} \quad (4.6)$$

with obvious notation. The Lagrangian \mathcal{L}_K is now chosen such that the tree-level amplitudes up to and including $\mathcal{O}(\epsilon^4)$ become (cf. Ref. [21], Eqs. (4.6), (4.7))

$$\begin{aligned} \mathcal{M}_N^{\text{tree}}(s_1, s_2, s_3) &= X_0 + X_1(s_3 - s_0^0) + X_2(s_3 - s_0^0)^2 + X_3(s_1 - s_2)^2, \\ \mathcal{M}_C^{\text{tree}}(s_1, s_2, s_3) &= Y_0 + Y_1(s_3 - s_0^+) + Y_2(s_3 - s_0^+)^2 + Y_3(s_1 - s_2)^2. \end{aligned} \quad (4.7)$$

We assume T -invariance and a hermitian \mathcal{L}_K , as a result of which the couplings X_i, Y_i are real. Expressing s_i through p_i^0 with the use of Eq. (4.4), these expressions are equivalent to

$$\begin{aligned} \mathcal{M}_N^{\text{tree}}(s_1, s_2, s_3) &= G_0 + G_1(p_3^0 - M_\pi) + G_2(p_3^0 - M_\pi)^2 + G_3(p_1^0 - p_2^0)^2, \\ \mathcal{M}_C^{\text{tree}}(s_1, s_2, s_3) &= H_0 + H_1(p_3^0 - M_\pi) + H_2(p_3^0 - M_\pi)^2 + H_3(p_1^0 - p_2^0)^2, \end{aligned} \quad (4.8)$$

where

$$\begin{aligned} G_0 &= X_0 + ((M_K - M_\pi)^2 - s_0^0)X_1 + ((M_K - M_\pi)^2 - s_0^0)^2 X_2, \\ G_1 &= -2M_K X_1 - 4M_K((M_K - M_\pi)^2 - s_0^0)X_2, \quad G_2 = 4M_K^2 X_2, \quad G_3 = 4M_K^2 X_3, \\ H_0 &= Y_0 + ((M_K - M_\pi)^2 - s_0^+)Y_1 + ((M_K - M_\pi)^2 - s_0^+)^2 Y_2, \\ H_1 &= -2M_K Y_1 - 4M_K((M_K - M_\pi)^2 - s_0^+)Y_2, \quad H_2 = 4M_K^2 Y_2, \quad H_3 = 4M_K^2 Y_3. \end{aligned} \quad (4.9)$$

From the expressions Eq. (4.8) one may read off the pertinent Lagrangian,

$$\begin{aligned} \mathcal{L}_K &= K^\dagger 2W_K(i\partial_t - W_K)K + \frac{G_0}{2} (K^\dagger \Phi_+ \Phi_0^2 + h.c.) + \frac{G_1}{2} (K^\dagger (W_+ - M_\pi) \Phi_+ \Phi_0^2 + h.c.) \\ &+ \frac{G_2}{2} (K^\dagger (W_+ - M_\pi)^2 \Phi_+ \Phi_0^2 + h.c.) + G_3 (K^\dagger \Phi_+ (W_0^2 \Phi_0 \Phi_0 - W_0 \Phi_0 W_0 \Phi_0) + h.c.) \\ &+ \frac{H_0}{2} (K^\dagger \Phi_- \Phi_+^2 + h.c.) + \frac{H_1}{2} (K^\dagger (W_- - M_\pi) \Phi_- \Phi_+^2 + h.c.) \\ &+ \frac{H_2}{2} (K^\dagger (W_- - M_\pi)^2 \Phi_- \Phi_+^2 + h.c.) + H_3 (K^\dagger \Phi_- (W_+^2 \Phi_+ \Phi_+ - W_+ \Phi_+ W_+ \Phi_+) + h.c.) + \dots, \end{aligned} \quad (4.10)$$

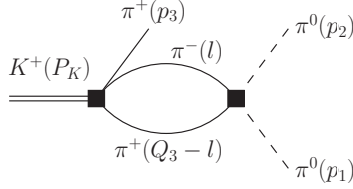


Figure 2: One-loop graph with derivative vertices (denoted by filled squares), with $Q_3^\mu = (p_1 + p_2)^\mu$.

where K denotes the non-relativistic field for the K^+ meson, $W_K = (M_K^2 - \Delta)^{1/2}$, and the ellipsis stands for higher-order terms in ϵ . Note that, by construction, the above Lagrangian contains all terms up to and including $O(\epsilon^4)$, allowed by the symmetries in the non-relativistic effective theory.

5. $K^+ \rightarrow 3\pi$ decays: pion rescattering to one loop

Here, we discuss terms of $O(a)$, generated by one-loop graphs of the type $\mathcal{L}_K \times \mathcal{L}_{\pi\pi}$, see Fig. 2 for a specific example. The technique used for the calculation of these loops is described in Sect. 2 for the case of non-derivative couplings. The presence of the latter does not change the procedure fundamentally, as we demonstrate for one specific example. Consider the diagram shown in Fig. 2. We restrict ourselves to the part of the amplitude proportional to the coupling H_1 , which can be written as

$$\mathcal{M}_N^{H_1}(s_1, s_2, s_3) = 2H_1(C_x + D_x(s_3 - \bar{s}_x)) \int \frac{d^d l}{(2\pi)^d} \frac{w(\mathbf{l}) - M_\pi}{2w(\mathbf{l})2w(\mathbf{Q}_3 - \mathbf{l})(w(\mathbf{l}) + w(\mathbf{Q}_3 - \mathbf{l}) - Q_3^0)}, \quad (5.1)$$

with $Q_3^\mu = (p_1 + p_2)^\mu$. Rewriting the numerator of the integrand as

$$w(\mathbf{l}) - M_\pi = \left(\frac{Q_3^0}{2} - M_\pi\right) + \frac{1}{2}(w(\mathbf{l}) + w(\mathbf{Q}_3 - \mathbf{l}) - Q_3^0) + \frac{1}{2}(w(\mathbf{l}) - w(\mathbf{Q}_3 - \mathbf{l})), \quad (5.2)$$

we see that only the first term yields a non-vanishing contribution after the integration, since the second term after expansion in momenta leads to dimensionally regularized no-scale integrals, and the third term is antisymmetric with respect to $\mathbf{l} \rightarrow \mathbf{Q}_3 - \mathbf{l}$. We finally obtain

$$\mathcal{M}_N^{H_1}(s_1, s_2, s_3) = 2H_1\left(\frac{Q_3^0}{2} - M_\pi\right)(C_x + D_x(s_3 - \bar{s}_x))J_{+-}(s_3), \quad (5.3)$$

where the function $J_{+-}(s_3)$ is given in Eq. (3.6).

The generalization to other derivative couplings is obvious. The complete one-loop representation for the decay amplitudes \mathcal{M}_N and \mathcal{M}_C , up-to-and-including terms of $O(a\epsilon^5)$, reads

$$\begin{aligned} \mathcal{M}_N^{(1\text{-loop})}(s_1, s_2, s_3) &= B_{N1}(s_3)J_{+-}(s_3) + B_{N2}(s_3)J_{00}(s_3) + \{B_{N3}(s_1, s_2, s_3)J_{+0}(s_1) + (s_1 \leftrightarrow s_2)\}, \\ \mathcal{M}_C^{(1\text{-loop})}(s_1, s_2, s_3) &= B_{C1}(s_3)J_{++}(s_3) + \{B_{C2}(s_1, s_2, s_3)J_{+-}(s_1) + B_{C3}(s_1)J_{00}(s_1) + (s_1 \leftrightarrow s_2)\}, \end{aligned} \quad (5.4)$$

where

$$\begin{aligned}
B_{N1}(s_3) &= 2[C_x + D_x(s_3 - \bar{s}_x) + F_x(s_3 - \bar{s}_x)^2] \left\{ H_0 + H_1 \left(\frac{Q_3^0}{2} - M_\pi \right) \right. \\
&\quad \left. + H_2 \left[\left(\frac{Q_3^0}{2} - M_\pi \right)^2 + \frac{Q_3^2}{12} \left(1 - \frac{4M_\pi^2}{s_3} \right) \right] + H_3 \left[\left(\frac{Q_3^0}{2} - p_3^0 \right)^2 + \frac{Q_3^2}{12} \left(1 - \frac{4M_\pi^2}{s_3} \right) \right] \right\}, \\
B_{N2}(s_3) &= [C_{00} + D_{00}(s_3 - \bar{s}_{00}) + F_{00}(s_3 - \bar{s}_{00})^2] \left\{ G_0 + G_1(p_3^0 - M_\pi) \right. \\
&\quad \left. + G_2(p_3^0 - M_\pi)^2 + G_3 \frac{Q_3^2}{3} \left(1 - \frac{4M_\pi^2}{s_3} \right) \right\}, \\
B_{N3}(s_1, s_2, s_3) &= 2[C_{+0} + D_{+0}(s_1 - \bar{s}_{+0}) + F_{+0}(s_1 - \bar{s}_{+0})^2] \left\{ G_0 + G_1 \left[\frac{Q_1^0}{2} \left(1 + \frac{\Delta_\pi}{s_1} \right) - M_\pi \right] \right. \\
&\quad \left. + G_2 \left[\left(\frac{Q_1^0}{2} \left(1 + \frac{\Delta_\pi}{s_1} \right) - M_\pi \right)^2 + \frac{Q_1^2}{12s_1^2} \lambda(s_1, M_\pi^2, M_{\pi^0}^2) \right] \right. \\
&\quad \left. + G_3 \left[\left(\frac{Q_1^0}{2} \left(1 - \frac{\Delta_\pi}{s_1} \right) - p_1^0 \right)^2 + \frac{Q_1^2}{12s_1^2} \lambda(s_1, M_\pi^2, M_{\pi^0}^2) \right] \right\} \\
&\quad - \frac{1}{3} E_{+0} \frac{q_{23}^2(s_1)}{M_K} \left[s_3 - s_2 + \frac{\Delta_\pi}{s_1} (M_K^2 - M_{\pi^0}^2) \right] \\
&\quad \times \left\{ G_1 + G_2 \left[\left(1 + \frac{\Delta_\pi}{s_1} \right) Q_1^0 - 2M_\pi \right] + G_3 \left[2p_1^0 - \left(1 - \frac{\Delta_\pi}{s_1} \right) Q_1^0 \right] \right\} + \mathcal{O}(\Delta_\pi^2), \quad (5.5)
\end{aligned}$$

and

$$\begin{aligned}
B_{C1}(s_3) &= [C_{++} + D_{++}(s_3 - \bar{s}_{++}) + F_{++}(s_3 - \bar{s}_{++})^2] \left\{ H_0 + H_1(p_3^0 - M_\pi) \right. \\
&\quad \left. + H_2(p_3^0 - M_\pi)^2 + H_3 \frac{Q_3^2}{3} \left(1 - \frac{4M_\pi^2}{s_3} \right) \right\}, \\
B_{C2}(s_1, s_2, s_3) &= 2[C_{+-} + D_{+-}(s_1 - \bar{s}_{+-}) + F_{+-}(s_1 - \bar{s}_{+-})^2] \left\{ H_0 + H_1 \left[\frac{Q_1^0}{2} - M_\pi \right] \right. \\
&\quad \left. + H_2 \left[\left(\frac{Q_1^0}{2} - M_\pi \right)^2 + \frac{Q_1^2}{12} \left(1 - \frac{4M_\pi^2}{s_1} \right) \right] + H_3 \left[\left(\frac{Q_1^0}{2} - p_1^0 \right)^2 + \frac{Q_1^2}{12} \left(1 - \frac{4M_\pi^2}{s_1} \right) \right] \right\} \\
&\quad - \frac{1}{3} E_{+-} \frac{q_{23}^2(s_1)}{M_K} (s_3 - s_2) \left\{ H_1 + H_2[Q_1^0 - 2M_\pi] + H_3[2p_1^0 - Q_1^0] \right\}, \\
B_{C3}(s_1) &= [C_x + D_x(s_1 - \bar{s}_x) + F_x(s_1 - \bar{s}_x)^2] \left\{ G_0 + G_1(p_1^0 - M_\pi) \right. \\
&\quad \left. + G_2(p_1^0 - M_\pi)^2 + G_3 \frac{Q_1^2}{3} \left(1 - \frac{4M_\pi^2}{s_1} \right) \right\}. \quad (5.6)
\end{aligned}$$

Here we have added terms of $\mathcal{O}(\epsilon^4)$ ($\propto F_i$, in a canonical extension of our notation) to the $\pi\pi$ amplitudes, without having them formally introduced on the Lagrangian level. They contribute terms of order $(s - \bar{s})^2$ to the S-waves. Only some terms of $\mathcal{O}(\Delta_\pi^2)$ have been neglected in Eq. (5.5). Note in particular that there are no contributions of $\pi\pi$ D-waves at this order.

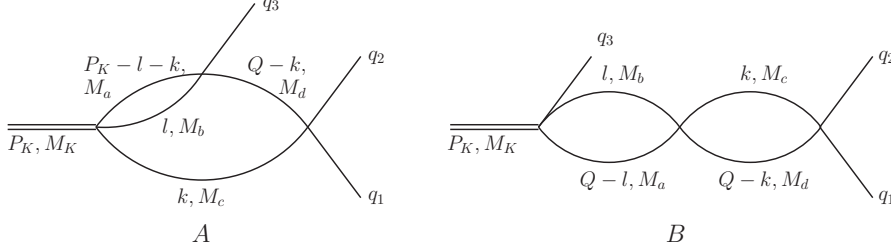


Figure 3: Two topologically distinct non-relativistic two-loop graphs describing the final-state $\pi\pi$ rescattering in the decay $K \rightarrow 3\pi$, with $Q^\mu = q_1^\mu + q_2^\mu$. The positions of the leading Landau singularities of graph A are discussed in Appendix F.

6. $K^+ \rightarrow 3\pi$ decays: pion rescattering to two loops

6.1. The diagrams

There are two topologically distinct two-loop graphs that describe pion-pion rescattering in the final state, see Fig. 3. In order to ease notation, we set $Q^\mu \doteq q_1^\mu + q_2^\mu$, $s \doteq Q^2$. Further,

$$Q^0 = \frac{M_K^2 + s - q_3^2}{2M_K}, \quad \mathbf{Q}^2 = \frac{\lambda(M_K^2, s, q_3^2)}{4M_K^2}. \quad (6.1)$$

In addition, throughout this chapter we consider the case of the non-derivative couplings only. In this case, in the rest frame of the kaon it is possible to express both diagrams shown in Fig. 3 in terms of a single variable s and one has

$$\mathcal{M}_{N,C}^{2\text{-loops}}(s) = \mathcal{M}_{N,C}^A(s) + \mathcal{M}_{N,C}^B(s). \quad (6.2)$$

The diagram in Fig. 3B, apart from the prefactor containing coupling constants, is given by a trivial product of two one-loop diagrams, which were already given in Eq. (3.6),

$$\mathcal{M}_{N,C}^B(s) \propto J_{ab}(s)J_{cd}(s). \quad (6.3)$$

Obviously, in the non-relativistic framework $\mathcal{M}_{N,C}^B(s)$ is therefore ultraviolet finite and of order ϵ^2 .

In the remaining part of this section we discuss the evaluation of the non-trivial contribution $\mathcal{M}_{N,C}^A(s)$, which stems from Fig. 3A. It is in particular shown that – up to a low-energy polynomial and an imaginary part which does not contribute at the accuracy we are working – $\mathcal{M}_{N,C}^A(s)$ is given by the function $F(M_a, M_b, M_c, M_d; s)$ defined in Eq. (6.23). So, the reader not interested in the details of the derivation may directly proceed to Eq. (6.23).

6.2. Evaluation of the generic two-loop function

The quantity $\mathcal{M}_{N,C}^A(s)$ is proportional to the generic two-loop function

$$\begin{aligned} \mathcal{M}(s) = & \int \frac{d^D l}{(2\pi)^{D_i}} \frac{d^D k}{(2\pi)^{D_i}} \frac{1}{2w_a(-\mathbf{l} - \mathbf{k})} \frac{1}{w_a(-\mathbf{l} - \mathbf{k}) - M_K + l^0 + k^0} \frac{1}{2w_b(\mathbf{l})} \frac{1}{w_b(\mathbf{l}) - l^0} \\ & \times \frac{1}{2w_c(\mathbf{k})} \frac{1}{w_c(\mathbf{k}) - k^0} \frac{1}{2w_d(\mathbf{Q} - \mathbf{k})} \frac{1}{w_d(\mathbf{Q} - \mathbf{k}) - Q^0 + k^0}. \end{aligned} \quad (6.4)$$

Performing the integration over the fourth components of the momenta, we can rewrite the above integral in the rest frame of the kaon as

$$\mathcal{M}(s) = \int \frac{d^d k}{(2\pi)^d} \frac{1}{2w_c(\mathbf{k})2w_d(\mathbf{Q}-\mathbf{k})} \frac{J_{ab}(M_K - w_c(\mathbf{k}), -\mathbf{k})}{w_c(\mathbf{k}) + w_d(\mathbf{Q}-\mathbf{k}) - Q_0}, \quad (6.5)$$

where $J_{ab}(L_0, \mathbf{L})$ denotes the inner one-loop integral

$$J_{ab}(L_0, \mathbf{L}) = \int \frac{d^d l}{(2\pi)^d} \frac{1}{2w_a(\mathbf{L}-\mathbf{l})2w_b(\mathbf{l})} \frac{1}{w_a(\mathbf{L}-\mathbf{l}) + w_b(\mathbf{l}) - L_0}. \quad (6.6)$$

In the calculation of the inner integral, we proceed as in the case of equal masses, see Eqs. (2.5)–(2.9): we first shift the integration variable according to

$$\mathbf{l} \rightarrow \mathbf{l} + \frac{1}{2}(1 + \delta_L)\mathbf{L}, \quad \delta_L = -\frac{M_a^2 - M_b^2}{L^2}, \quad L^2 = (L^0)^2 - \mathbf{L}^2. \quad (6.7)$$

Further, using the identity

$$\begin{aligned} & \frac{1}{4w_a w_b} \left\{ -\frac{1}{L_0 - w_a - w_b} - \frac{1}{L^0 + w_a + w_b} + \frac{1}{L^0 + w_a - w_b} + \frac{1}{L^0 - w_a + w_b} \right\} \\ &= \frac{1}{2L^0} \frac{1}{\mathbf{l}^2 - (\mathbf{L}/L^0)^2 - k_0^2}, \end{aligned} \quad (6.8)$$

where

$$w_a = \sqrt{M_a^2 + \left(\frac{1}{2}(1 - \delta_L)\mathbf{L} - \mathbf{l}\right)^2}, \quad w_b = \sqrt{M_b^2 + \left(\frac{1}{2}(1 + \delta_L)\mathbf{L} + \mathbf{l}\right)^2}, \quad k_0^2 = \frac{\lambda(L^2, M_a^2, M_b^2)}{4L^2}, \quad (6.9)$$

applying threshold expansion and rescaling the component l_1 (see the discussion after Eq. (2.8)), we find

$$J_{ab}(L^0, \mathbf{L}) = \frac{1}{2\sqrt{L^2}} \int \frac{d^d l}{(2\pi)^d} \frac{1}{\mathbf{l}^2 - k_0^2}. \quad (6.10)$$

Finally, performing the \mathbf{l} integration, we reproduce Eq. (3.6) in the limit $d \rightarrow 3$.

In the two-loop diagram Eq. (6.5) the components of the momentum L^μ , corresponding to the one-loop subdiagram, are equal to $L^0 = M_K - w_c(\mathbf{k})$ and $\mathbf{L} = -\mathbf{k}$. One may further ensure that $k_0^2 = A_k(\Delta^2 - \mathbf{k}^2)$, where the quantities Δ^2 and A_k are given by

$$\begin{aligned} \Delta^2 &= \frac{\lambda(M_K^2, M_c^2, (M_a + M_b)^2)}{4M_K^2}, \quad A_k = \frac{M_K^2}{2(M_K^2 + M_c^2) - (M_a + M_b)^2 - s_k} \left(1 - \frac{(M_a - M_b)^2}{s_k}\right), \\ s_k &= M_K^2 + M_c^2 - 2M_K w_c(\mathbf{k}). \end{aligned} \quad (6.11)$$

Rescaling $\mathbf{l} \rightarrow (A_k)^{1/2}\mathbf{l}$, we finally arrive at

$$J_{ab}(M_K - w_c(\mathbf{k}), -\mathbf{k}) = \frac{A_k^{d/2-1}}{2\sqrt{s_k}} \int \frac{d^d l}{(2\pi)^d} \frac{1}{\mathbf{l}^2 + \mathbf{k}^2 - \Delta^2}. \quad (6.12)$$

Now we have to insert the above expression into Eq. (6.5) and calculate the two-loop integral. To this end, we rewrite the denominators in the outer loop, using again Eq. (6.8) with

$w_a, w_b \rightarrow w_d, w_c$ and $L^\mu \rightarrow Q^\mu$. The integral over the last three terms does not vanish any more in dimensional regularization, since these are multiplied by the inner loop, which is not a low-energy polynomial. It can however be easily checked that, expanding everything but the non-polynomial factor $(\mathbf{l}^2 + \mathbf{k}^2 - \Delta^2)^{-1}$ coming from the inner loop, one obtains a result of the form $P(s) = \tilde{P}(s)(-\Delta^2 - i\epsilon)^{d-2}$, where $\tilde{P}(s)$ is a low-energy polynomial in the variable s with real coefficients and a simple pole in $d - 3$. Consequently,

$$\mathcal{M}(s) = \frac{1}{2Q^0} \int \frac{d^d l}{(2\pi)^d} \frac{d^d k}{(2\pi)^d} \frac{A_k^{d/2-1}}{2\sqrt{s_k}} \frac{1}{\mathbf{l}^2 + \mathbf{k}^2 - \Delta^2} \frac{1}{\mathbf{p}^2 - (\mathbf{p}\mathbf{Q}/Q^0)^2 - q_0^2} + P(s) \doteq \bar{\mathcal{M}}(s) + P(s), \quad (6.13)$$

where $\mathbf{k} = \mathbf{p} + \frac{1}{2}(1 + \delta)\mathbf{Q}$, and

$$q_0^2 = \frac{\lambda(s, M_c^2, M_d^2)}{4s}, \quad \delta = \frac{M_c^2 - M_d^2}{s}. \quad (6.14)$$

6.3. Renormalization

At this stage, it is appropriate to discuss the freedom in the definition of $\mathcal{M}(s)$. For example, one may add an arbitrary low-energy polynomial of s with *real* coefficients to $\mathcal{M}(s)$ – this would amount to a renormalization of the $K \rightarrow 3\pi$ vertices G_i, H_i in the non-relativistic effective Lagrangian. One may use this freedom to remove the *real part* of the polynomial $P(s)$, which is of order a^2 and which contains an ultraviolet pole at $d = 3$.⁴ On the contrary, the imaginary part can not be removed in this manner. So if the imaginary part of $P(s)$ were divergent at $d \rightarrow 3$, it would constitute a major problem for the validity of the framework. However, this does not happen: as can be easily seen, the imaginary part is ultraviolet-finite. Moreover, at the accuracy we are working, one may neglect this imaginary part altogether, because its contribution to the decay rate starts at order a^3 , that is beyond the scope of the present paper.

To summarize, the two-loop function $\mathcal{M}(s)$ at the accuracy we are working can be replaced everywhere by

$$F(M_a, M_b, M_c, M_d; s) = \bar{\mathcal{M}}(s) - \text{Re } \bar{\mathcal{M}}(s), \quad (6.15)$$

where $s_t = (M_c + M_d)^2$. Here, we used the above-mentioned freedom to normalize the real part of $F(M_a, M_b, M_c, M_d; s)$ to zero at $s = s_t$. The difference between F and \mathcal{M} is a low-energy polynomial. The real part of this polynomial can be removed by renormalization, and the imaginary part is ultraviolet-finite and does not contribute at the required precision.

6.4. Integral representation

The rest of this section is devoted to the calculation of the function F . After shifting the integration variable in Eq. (6.13) according to

$$\mathbf{k} \rightarrow \mathbf{k} + \left(\frac{\mathbf{k}\mathbf{Q}}{Q^2} \left(\frac{Q^0}{\sqrt{s}} - 1 \right) + \frac{1 + \delta}{2} \right) \mathbf{Q}, \quad (6.16)$$

we arrive at

$$\bar{\mathcal{M}}(s) = \frac{1}{2\sqrt{s}} \int \frac{d^d l}{(2\pi)^d} \frac{d^d k}{(2\pi)^d} \frac{1}{(\mathbf{k}^2 - q_0^2)} \frac{N(x)}{(\mathbf{l}^2 + \frac{(1+\delta)^2}{4} \mathbf{Q}^2 + x - \Delta^2)}, \quad (6.17)$$

⁴Renormalization of the couplings G_i, H_i first occurs at two-loop order in our framework.

where

$$x = \mathbf{k}^2 + \frac{(\mathbf{k}\mathbf{Q})^2}{s} + \frac{\mathbf{k}\mathbf{Q}}{\sqrt{s}} \mathcal{Q}^0(1 + \delta), \quad N(x) = \frac{A_k^{d/2-1}(s_k(x))}{2\sqrt{s_k(x)}},$$

$$s_k(x) = M_K^2 + M_c^2 - 2M_K \left(M_c^2 + \frac{(1 + \delta)^2}{4} \mathbf{Q}^2 + x \right)^{1/2}. \quad (6.18)$$

In order to evaluate the integral in Eq. (6.17), we expand the numerator $N(x)$ in the variable x and integrate term by term. Using Feynman parameterization to combine the two denominators, we obtain

$$\bar{M}(s) = \frac{1}{2\sqrt{s}} \sum_{n=0}^{\infty} \frac{1}{n!} \frac{d^n}{dx^n} N(x) \Big|_{x=0} J_n(s),$$

$$J_n(s) = \frac{\Gamma(2-d)}{(4\pi)^d} \int_0^1 dy y^{-d/2} \left(1 + \frac{y\mathbf{Q}^2}{s} \right)^{-1/2} f_d^{(n)}(y, s) (g(y, s) - i\epsilon)^{d-2}, \quad (6.19)$$

where $g(y, s)$ is defined by

$$g(y, s) = -(1-y)q_0^2 - y\Delta^2 + \frac{\frac{1}{4}y(1-y)\mathbf{Q}^2(1+\delta)^2}{1 + \frac{y\mathbf{Q}^2}{s}}, \quad (6.20)$$

and the first few coefficients in the expansion are given by

$$f_d^{(0)}(y, s) = 1, \quad f_d^{(1)}(y, s) = \frac{dg(y, s)}{2(1-d)} \left(1 + \frac{\mathbf{Q}^2\alpha}{ds} \right) + \gamma, \quad (6.21)$$

$$f_d^{(2)}(y, s) = -\frac{(2+d)g^2(y, s)}{4(1-d)} \left(1 + \frac{2\mathbf{Q}^2\alpha}{ds} + \frac{3\mathbf{Q}^4\alpha^2}{d(d+2)s^2} \right) + \frac{dg(y, s)}{2(1-d)} \left(2\gamma + \frac{\mathbf{Q}^2(2\alpha\gamma + \beta^2 s)}{ds} \right) + \gamma^2.$$

Here,

$$\alpha = \frac{1-y}{1 + \frac{y\mathbf{Q}^2}{s}}, \quad \beta = \frac{\alpha\mathcal{Q}^0}{\sqrt{s}}(1+\delta) \frac{1}{\sqrt{1 + \frac{y\mathbf{Q}^2}{s}}}, \quad \gamma = -\frac{\mathbf{Q}^2(\mathcal{Q}^0)^2}{2s} y(1+\delta)^2 \frac{1 - \frac{y}{2} \left(1 - \frac{\mathbf{Q}^2}{s} \right)}{\left(1 + \frac{y\mathbf{Q}^2}{s} \right)^2}. \quad (6.22)$$

In order to eliminate the singularity at $y = 0$ when $d \rightarrow 3$, we first integrate by parts and omit the surface term, which is a low-energy polynomial in s . One may further verify that in the limit $d \rightarrow 3$, up to a low-energy polynomial, the function F is given by the following integral representation

$$F(M_a, M_b, M_c, M_d; s) = \frac{1}{256\pi^3 \sqrt{s}} \int_0^1 \frac{dy}{\sqrt{y}} \mathcal{F}(y, s) (\ln g(y, s) - \ln g(y, s_t)). \quad (6.23)$$

The function $\mathcal{F}(y, s)$ is given by an infinite sum

$$\mathcal{F}(y, s) = \sum_{n=0}^{\infty} \mathcal{F}_n(y, s), \quad \mathcal{F}_n(y, s) = \frac{4}{n!} \frac{d^n}{dx^n} N(x) \Big|_{x=0} \frac{d}{dy} \left(\frac{g(y, s) f^{(n)}(y, s)}{\sqrt{1 + \frac{y\mathbf{Q}^2}{s}}} \right) = \mathcal{O}(\epsilon^{2n+2}), \quad (6.24)$$

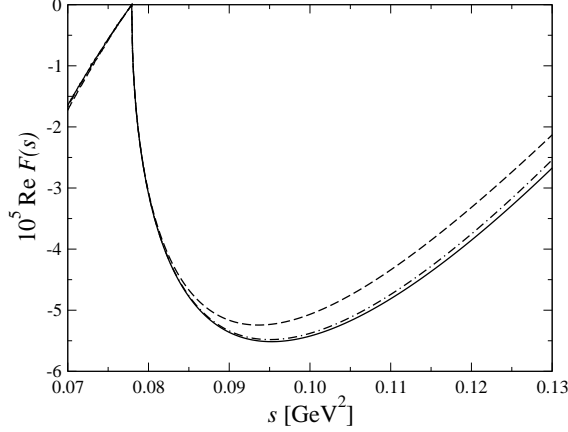


Figure 4: Successive approximations for $\text{Re } F(M_\pi, M_\pi, M_\pi, M_\pi; s) \doteq \text{Re } F(s)$ in the equal-mass case. We show the leading-order (maximum $n = 0$, dashed), next-to-leading-order ($n = 1$, dash-dotted), and next-to-next-to-leading-order ($n = 2$, full line) approximations, see Eq. (6.24).

and $f^{(n)}(y, s) = f_d^{(n)}(y, s)|_{d=3}$. In particular, for $n = 0$ we find

$$\mathcal{F}_0(y, s) = \frac{\lambda^{1/2}(s_0, M_a^2, M_b^2)}{s_0} \frac{1}{\sqrt{\Delta^2 - \frac{(1+\delta)^2}{4} \mathbf{Q}^2}} \frac{d}{dy} \left(\frac{g(y, s)}{\sqrt{1 + \frac{y\mathbf{Q}^2}{s}}} \right), \quad (6.25)$$

where

$$s_0 = M_K^2 + M_c^2 - 2M_K \sqrt{M_c^2 + \frac{\mathbf{Q}^2}{4} (1 + \delta)^2}. \quad (6.26)$$

The series in n for the function $F(M_a, M_b, M_c, M_d; s)$ converges rapidly: we display the successive approximations with maximum $n = 0, 1, 2$ for the equal-mass case in Fig. 4. It is seen that there is almost no difference between the two approximations with maximum $n = 1$ and $n = 2$.

The function $F(M_a, M_b, M_c, M_d; s)$ given by Eq. (6.23) starts at $\mathcal{O}(\epsilon^2)$ and thus does not violate power counting. Note also that, expanding the function \mathcal{F} in powers of $\frac{y\mathbf{Q}^2}{s} = \mathcal{O}(\epsilon^2)$, it is possible to perform the integrals in y analytically at each order. The result at next-to-leading order is given in Appendix B. Analytic properties of this function are considered in Appendix C, and the comparison to the relativistic approach is discussed in Appendix G.

6.5. Threshold behavior

Finally, we display the singularity structure of the function $F(M_a, M_b, M_c, M_d; s)$ near the cusp. It can be shown that

$$F(M_a, M_b, M_c, M_d; s) = \frac{i\lambda^{1/2}(s, M_c^2, M_d^2)}{16\pi s} \frac{i\lambda^{1/2}(s_{0t}, M_a^2, M_b^2)}{16\pi s_{0t}} + \mathcal{O}(q_0^2), \quad (6.27)$$

where s_{0t} denotes the function $s_0(s)$ in Eq. (6.26), evaluated at $s = s_t$. Hence in the vicinity of the cusp, the two-loop diagram is given as a product of two factors: the first factor describes the cusp emerging in the outer loop, while the second factor is the inner loop evaluated at the threshold $s = 4M_\pi^2$. Thus, the above two-loop diagram satisfies the threshold theorem [1, 21, 22, 23, 24].

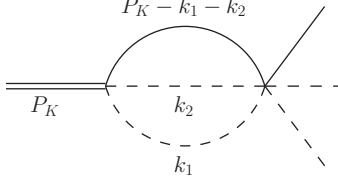


Figure 5: A non-relativistic two-loop graph describing the decay $K^+ \rightarrow \pi^0 \pi^0 \pi^+$ that involves a six-particle vertex. The intermediate state contains the particles $\pi^0(k_1)$, $\pi^0(k_2)$, and $\pi^+(P_K - k_1 - k_2)$.

7. Three-pion couplings

Pion rescattering in the final state also contains a contribution from diagrams of the type shown in Fig. 5. These diagrams contain a vertex describing the interaction of six pions at the same point. In the non-relativistic theory, such interactions are generated by a Lagrangian of the type

$$\mathcal{L}_{3\pi} = \frac{1}{4} F_0 \Phi_+^\dagger (\Phi_0^\dagger)^2 \Phi_+ \Phi_0^2 + \frac{1}{4} F_0' \Phi_-^\dagger (\Phi_+^\dagger)^2 \Phi_- \Phi_+^2 + \dots, \quad (7.1)$$

where the ellipsis stands for terms with space derivatives.

For demonstration, let us consider the diagram with a $\pi^0 \pi^0 \pi^+$ intermediate state, depicted in Fig. 5. The contribution of this diagram to the decay amplitude \mathcal{M}_N is a constant, which in the center-of-mass frame of the kaon $P_K = (M_K, \mathbf{0})$ is given by

$$\begin{aligned} \mathcal{M}_N^{3\pi}(s_1, s_2, s_3) &= \frac{1}{2} G_0 F_0 \int \frac{d^d k_1}{(2\pi)^d} \int \frac{d^d k_2}{(2\pi)^d} \frac{1}{2w_0(\mathbf{k}_1)} \frac{1}{2w_0(\mathbf{k}_2)} \\ &\quad \times \frac{1}{2w(\mathbf{k}_1 + \mathbf{k}_2)} \frac{1}{w_0(\mathbf{k}_1) + w_0(\mathbf{k}_2) + w(\mathbf{k}_1 + \mathbf{k}_2) - M_K}. \end{aligned} \quad (7.2)$$

Obviously, the diagram is a constant. Its real part, which is in fact divergent for $d \rightarrow 3$, can therefore be absorbed in a redefinition of the coupling constant G_0 , and will not be considered further. We concentrate on the finite imaginary part, for which we may take $d \rightarrow 3$ and rewrite the above expression in the relativistically covariant manner

$$\begin{aligned} \text{Im } \mathcal{M}_N^{3\pi}(s_1, s_2, s_3) &= \frac{i}{128\pi^5} G_0 F_0 \int \prod_{i=1}^3 d^4 k_i \theta(k_i^0) \delta(k_i^2 - M_i^2) \delta^{(4)}(P_K - k_1 - k_2 - k_3) \\ &= \frac{i G_0 F_0 (M_K - 3M_\pi)^2}{768 \sqrt{3}\pi^2} + \mathcal{O}(\Delta_\pi, (M_K - 3M_\pi)^3). \end{aligned} \quad (7.3)$$

Similar to Ref. [21], for the rough estimate of the magnitude of the coupling F_0 we use matching to chiral perturbation theory. At lowest order this results in

$$F_0 = \frac{M_\pi^2}{8F_\pi^4} + \dots, \quad (7.4)$$

where the ellipsis stands for higher chiral orders, and $F_\pi = 92.2$ MeV is the pion decay constant. Since also the imaginary part of the diagram in Fig. 5 is a constant, it is possible to eliminate this contribution by allowing the constant G_0 to have a small imaginary part

$$\frac{\text{Im } G_0}{\text{Re } G_0} \simeq \frac{(M_K - 3M_\pi)^2}{768 \sqrt{3}\pi^2} \frac{M_\pi^2}{8F_\pi^4} \simeq 1.5 \cdot 10^{-5}. \quad (7.5)$$

Note that Eq. (7.5) does not contain effects from the $\pi^+\pi^+\pi^-$ intermediate state, which would contribute a similar term $\propto H_0/G_0$. As the effect turns out to be so small, we will neglect it below and continue to assume that the couplings in the non-relativistic kaon effective Lagrangian are real. Note that our result is in qualitative agreement with Eq. (80) of Ref. [21], although the exact coefficients differ.

We wish to stress that the non-relativistic theory without six-particle couplings is in general not self-consistent (see, e.g., Ref. [44]). The reason for this is that there exist divergent two-loop graphs for the process $3\pi \rightarrow 3\pi$ that require the introduction of a six-particle counterterm in the Lagrangian. These diagrams arise, however, at order a^4 in the expansion in (small) $\pi\pi$ scattering lengths and thus are beyond the scope of the present article.

8. $K^+ \rightarrow 3\pi$ decay amplitudes to two loops: final result

In order to find the representation of the decay amplitudes at $O(a^2)$, we draw all possible graphs for $K^+ \rightarrow \pi^0\pi^0\pi^+$ and $K^+ \rightarrow \pi^+\pi^+\pi^-$ at one- and two-loop order, comprising the topologies discussed in detail in Sects. 5 and 6; for an explicit display of the different pion intermediate states, see Refs. [22, 23]. Further, in the graphs of type Fig. 3A we retain only the non-analytic piece $F(M_a, M_b, M_c, M_d; s)$, whereas the (infinite) polynomial is included in the tree-level couplings G_i, H_i . The choice of the particular representation Eq. (6.23) is equivalent to the choice of a renormalization prescription. Note also that the resulting modification of G_i, H_i is of order a^2 , so that if one uses the modified couplings also to calculate one- and two-loop diagrams, the results change at $O(a^3)$ and $O(a^4)$, respectively, that is beyond the accuracy we consider.

The amplitudes up to and including two loops are given by

$$\begin{aligned} \mathcal{M}_{00+} &= \mathcal{M}_N^{\text{tree}} + \mathcal{M}_N^{1\text{-loop}} + \mathcal{M}_N^{2\text{-loops}} + \dots & [K^+ \rightarrow \pi^0\pi^0\pi^+], \\ \mathcal{M}_{++-} &= \mathcal{M}_C^{\text{tree}} + \mathcal{M}_C^{1\text{-loop}} + \mathcal{M}_C^{2\text{-loops}} + \dots & [K^+ \rightarrow \pi^+\pi^+\pi^-]. \end{aligned} \quad (8.1)$$

Our amplitudes are normalized such that the decay rates are given by

$$d\Gamma = \frac{1}{2M_K} (2\pi)^4 \delta^{(4)}(P_f - P_i) |\mathcal{M}|^2 \prod_{i=1}^3 \frac{d^3\mathbf{p}_i}{2(2\pi)^3 p_i^0}. \quad (8.2)$$

The tree-level contribution to the $K^+ \rightarrow \pi^0\pi^0\pi^+$ and $K^+ \rightarrow \pi^+\pi^+\pi^-$ decay amplitudes up to $O(\epsilon^4)$ is given by Eq. (4.8). The one-loop amplitude fully consistent up to $O(a\epsilon^5)$ is displayed in Eqs. (5.4), (5.5), and (5.6). Finally, the two-loop contributions to the amplitude, which are by far the lengthiest and most complicated part, are given explicitly in Appendix A. These are complete up to $O(a^2\epsilon^4)$, but contain partial terms of $O(a^2\epsilon^6)$ and $O(a^2\epsilon^8)$, retained for the following reason. As we have seen in Sect. 3.2, no reasonable description of the $\pi\pi$ S-wave scattering amplitudes is possible without including the effective ranges. We have therefore kept all linear energy dependences in the S-wave interactions, generating in combination terms up to $O(a^2\epsilon^8)$. In the two-loop graphs, we neglect however terms induced by couplings quadratic in energy ($\propto G_{2/3}, H_{2/3}, \pi\pi$ shape parameters) as well as higher orders in P- (or even D-)waves.

Prior to using this representation in the fit, one eliminates the coupling constants C_i, D_i, E_i in favor of the $\pi\pi$ threshold parameters through the matching conditions discussed in Sect. 3. This representation depends on the eight real $K \rightarrow 3\pi$ coupling constants H_i, G_i and the threshold parameters for $\pi\pi$ scattering, which in the end ought to be determined from a fit to the experimental

data. It is this amplitude, fully documented here for the first time, that, amended with the radiative corrections provided in Ref. [24], has been used in the analysis of the NA48/2 $K^+ \rightarrow \pi^0 \pi^0 \pi^+$ data [17], which in combination with results from K_{e4} decays led to the determination of $\pi\pi$ scattering lengths quoted in Eq. (1.2).

9. Comparison with other approaches

The low-energy expansion proposed here is closely related to early work performed in the 1960s by many authors, who used S -matrix methods to investigate the production of particles in the threshold region, in particular also in $K \rightarrow 3\pi$ decays. We refer the interested reader to the article by Anisovich and Ansel'm [45] for a review. The framework presented here may be considered an effective field theory realization of these approaches. The most notable differences are:

1. In these early approaches, the occurrence of a cusp in the decay rates went unnoticed.
2. It is explicitly stated in Ref. [45] that there are no leading Landau singularities in the graphs of the type Fig. 3A, which does not agree with what we find. As a result, our expressions for the two-loop integrals do not agree with the ones presented in these early articles.
3. Our approach allows for a straightforward inclusion of the effects of real and virtual photons, see Ref. [24] for the actual evaluation of the pertinent matrix elements, and Ref. [17] for applications in the data analysis of $K \rightarrow 3\pi$ decays.

A comparison of the present framework with the seminal articles of Cabibbo and Isidori [2, 21] was already provided in Ref. [22], and we refer to that article for details. Here we only recall that the decomposition of the decay amplitudes [2, 21] into the form $\mathcal{M} = \mathcal{M}_0 + v_{cd}(s)\mathcal{M}_1$, with $\mathcal{M}_{0,1}$ holomorphic, is valid near the threshold only, as is detailed in Appendix H. Furthermore, the leading Landau singularities found here were missed in Ref. [2, 21]. However, the analysis in Ref. [17] shows that, at the accuracy considered, these effects are immaterial for the main problem at hand, the extraction of the $\pi\pi$ scattering lengths from the cusp strength. Various aspects of $K \rightarrow 3\pi$ decays are presented in the recent articles Refs. [46, 47, 48, 49, 50, 51, 52, 53]. A comparison of these works with the present approach is provided in Refs. [22, 23, 24], see also Ref. [17] for a careful comparison of the results of Refs. [50, 51, 52] with those of Ref. [24]. We refer the interested reader to these articles for details.

A dispersive approach has recently been undertaken to $K \rightarrow 3\pi$ (and $\eta \rightarrow 3\pi$) decays [54, 55], and an analytical expression for the decay amplitudes for $K_L \rightarrow 3\pi$ valid up to two loops in chiral perturbation theory is already available. On the other hand, it seems to us that the effects of real and virtual photons are very difficult to incorporate without a Lagrangian framework. The main difference to the framework presented here is the fact that quark mass effects are treated in a perturbative manner in Refs. [54].

10. Summary and conclusions

We summarize the main findings of our investigations as follows.

1. $\pi\pi$ rescattering generates a cusp in the decay distribution of $K^\pm \rightarrow \pi^0 \pi^0 \pi^\pm$ decays and allows one to measure $\pi\pi$ S-wave scattering lengths a_0 and a_2 [1]. This cusp has been investigated in recent years by the NA48/2 collaboration in great detail [3, 16, 17], and the two scattering lengths were determined in this manner.

2. The analysis of the NA48/2 collaboration relies on two theoretical frameworks [21, 22, 23], which relate the decay distribution to the scattering lengths. In this article, we spell out details of the method that underlies the matrix elements worked out in Refs. [22, 23] and used in Ref. [17] for the data analysis.
3. We investigate the decays $K \rightarrow 3\pi$ within an approach which is based on non-relativistic effective Lagrangians. It enables one to systematically calculate the decay amplitudes $K^+ \rightarrow \pi^0\pi^0\pi^+$ and $K^+ \rightarrow \pi^+\pi^+\pi^-$ in a double expansion in small momenta of the decay products and in the threshold parameters of the $\pi\pi$ scattering (scattering lengths, etc.). Furthermore, it allows one to take into account radiative corrections in a standard manner [24].
4. Because it is a Lagrangian framework, the strictures of unitarity, analyticity and of the cluster decomposition are automatically taken into account. Furthermore, the amplitudes contain the Landau singularities automatically.
5. In this article, we provide the amplitudes for $K^\pm \rightarrow \pi^0\pi^0\pi^\pm$ and for $K^\pm \rightarrow \pi^\pm\pi^+\pi^-$ in closed form, at two-loop order, up to and including terms of order $a^2\epsilon^4$, with the most important terms of order $a^2\epsilon^6$ and $a^2\epsilon^8$ also retained. The extension to $K_L \rightarrow 3\pi$ decays is straightforward.

In conclusion, the framework presented here is very suitable to investigate the beautiful set of data on $K \rightarrow 3\pi$ decays collected by the NA48/2 collaboration – it has all the bells and whistles provided by quantum field theory. We expect that the empirical parameterization of the Dalitz plot distribution published recently [56] would even allow one to study the convergence of the a, ϵ expansion and to narrow down the emerging theoretical uncertainty in the scattering lengths $a_{0,2}$. This endeavour is, however, beyond the scope of this work.

Acknowledgments

We thank Gilberto Colangelo for collaboration at an early stage of this work, Sebastian Schneider for some independent checks, and Martin Zdráhal for useful discussions as well as extensive comments that helped us improve this manuscript. We enjoyed extensive conversations with and support from Brigitte Bloch-Devaux, Luigi DiLella, and Italo Mannelli concerning applications of the results presented here in the data analysis. We thank Thomas Hahn for generous help with using *LoopTools*, which we used to check some of our results on relativistic amplitudes. Partial financial support by the Helmholtz Association through funds provided to the virtual institute “Spin and strong QCD” (VH-VI-231), the project “Study of Strongly Interacting Matter” (HadronPhysics2, grant No. 227431) under the 7th Framework Programme of the EU, and by DFG (SFB/TR 16, “Subnuclear Structure of Matter”) is gratefully acknowledged. This work was supported by the Swiss National Science Foundation, and by EU MRTN-CT-2006-035482 (FLAVIANet). One of us (J.G.) is grateful to the Alexander von Humboldt-Stiftung and to the Helmholtz-Gemeinschaft for the award of a prize that allowed him to stay at the HISKP at the University of Bonn, where part of this work was performed. He also thanks the HISKP for the warm hospitality during these stays. A.R. acknowledges support by the Georgia National Science Foundation (grant No. GNSF/ST08/4-401).

Appendix A. $K^+ \rightarrow 3\pi$ amplitudes up to $\mathcal{O}(a^2\epsilon^4)$

We have calculated the two-loop contributions to the decay amplitudes for $K^+ \rightarrow \pi^0\pi^0\pi^+$ and $K^+ \rightarrow \pi^+\pi^+\pi^-$ including derivative couplings, along the lines explained in detail in Sect. 6. The results we find, complete at order $a^2\epsilon^4$ and containing additional terms of $\mathcal{O}(a^2\epsilon^6)$, $\mathcal{O}(a^2\epsilon^8)$ (see the comments in Sect. 8), read

$$\mathcal{M}_{N,C}^{2\text{-loops}} = \mathcal{M}_{N,C}^A(s_1, s_2, s_3) + \mathcal{M}_{N,C}^B(s_1, s_2, s_3), \quad (\text{A.1})$$

where

$$\begin{aligned} \mathcal{M}_N^A = & 4H_{+-}'''(s_3)C_{+-}(\tilde{s}_3^{+-})C_x(s_3)F_+(M_\pi, M_\pi, M_\pi, M_\pi; s_3) \\ & - 4\left[\frac{1}{2}H_1C_{+-}(\tilde{s}_3^{+-}) + 2M_KH_{+-}'''(s_3)D_{+-}\right]C_x(s_3)\frac{\mathbf{Q}_3^2}{Q_3^0}F_+^{(1)}(M_\pi, M_\pi, M_\pi, M_\pi; s_3) \\ & + 4M_KH_1D_{+-}C_x(s_3)\frac{\mathbf{Q}_3^4}{(Q_3^0)^2}F_+^{(2)}(M_\pi, M_\pi, M_\pi, M_\pi; s_3) \\ & + 2G''(s_3)C_x(\tilde{s}_3^{+-})C_x(s_3)F_+(M_{\pi^0}, M_{\pi^0}, M_\pi, M_\pi; s_3) \\ & + 2[G_1C_x(\tilde{s}_3^{+-}) - 2M_KG''(s_3)D_x]C_x(s_3)\frac{\mathbf{Q}_3^2}{Q_3^0}F_+^{(1)}(M_{\pi^0}, M_{\pi^0}, M_\pi, M_\pi; s_3) \\ & - 4M_KG_1D_xC_x(s_3)\frac{\mathbf{Q}_3^4}{(Q_3^0)^2}F_+^{(2)}(M_{\pi^0}, M_{\pi^0}, M_\pi, M_\pi; s_3) \\ & + 2H''(s_3)C_{++}(\tilde{s}_3^{+-})C_x(s_3)F_+(M_\pi, M_\pi, M_\pi, M_\pi; s_3) \\ & + 2[H_1C_{++}(\tilde{s}_3^{+-}) - 2M_KH''(s_3)D_{++}]C_x(s_3)\frac{\mathbf{Q}_3^2}{Q_3^0}F_+^{(1)}(M_\pi, M_\pi, M_\pi, M_\pi; s_3) \\ & - 4M_KH_1D_{++}C_x(s_3)\frac{\mathbf{Q}_3^4}{(Q_3^0)^2}F_+^{(2)}(M_\pi, M_\pi, M_\pi, M_\pi; s_3) \\ & + 4G_{+0}'''(s_3)C_{+0}(\tilde{s}_3^{00})C_{00}(s_3)F_+(M_\pi, M_{\pi^0}, M_{\pi^0}, M_{\pi^0}; s_3) \\ & - 4\left[\frac{1}{2}G_1C_{+0}(\tilde{s}_3^{00}) + 2M_KG_{+0}'''(s_3)D_{+0}\right]C_{00}(s_3)\frac{\mathbf{Q}_3^2}{Q_3^0}F_+^{(1)}(M_\pi, M_{\pi^0}, M_{\pi^0}, M_{\pi^0}; s_3) \\ & + 4M_KG_1D_{+0}C_{00}(s_3)\frac{\mathbf{Q}_3^4}{(Q_3^0)^2}F_+^{(2)}(M_\pi, M_{\pi^0}, M_{\pi^0}, M_{\pi^0}; s_3) \\ & + \left\{4H_{+-}'''(s_1^+)C_x(\tilde{s}_1^{+0})[C_{+0}(s_1) + E_{+0}^+(s_1, s_2, s_3)]F_0(M_\pi, M_\pi, M_\pi, M_{\pi^0}; s_1) \right. \\ & \quad \left. - 4\left[\left(\frac{1}{2}H_1C_x(\tilde{s}_1^{+0}) + 2M_KH_{+-}'''(s_1^+)D_x\right)C_{+0}(s_1)\frac{\mathbf{Q}_1^2}{Q_1^0} + 2H_{+-}'''(s_1^+)C_x(\tilde{s}_1^{+0})E_{+0}(s_1, s_2, s_3)\right] \right. \\ & \quad \left. \times F_0^{(1)}(M_\pi, M_\pi, M_\pi, M_{\pi^0}; s_1) \right. \\ & \quad \left. + 4M_KH_1D_xC_{+0}(s_1)\frac{\mathbf{Q}_1^4}{(Q_1^0)^2}F_0^{(2)}(M_\pi, M_\pi, M_\pi, M_{\pi^0}; s_1) \right. \\ & \quad \left. + 4G_{+0}'''(s_1^-)C_{+0}(\tilde{s}_1^{0+})[C_{+0}(s_1) - E_{+0}^-(s_1, s_2, s_3)]F_0(M_{\pi^0}, M_\pi, M_{\pi^0}, M_\pi; s_1) \right. \end{aligned}$$

$$\begin{aligned}
& -4 \left[\left(\frac{1}{2} G_1 C_{+0}(\tilde{s}_1^{0+}) + 2M_K G''_{+0}(\tilde{s}_1^-) D_{+0} \right) C_{+0}(s_1) \frac{\mathbf{Q}_1^2}{\mathcal{Q}_1^0} - 2G''_{+0}(\tilde{s}_1^-) C_{+0}(\tilde{s}_1^{0+}) E_{+0}(s_1, s_2, s_3) \right] \\
& \quad \times F_0^{(1)}(M_{\pi^0}, M_\pi, M_{\pi^0}, M_\pi; s_1) \\
& + 4M_K G_1 D_{+0} C_{+0}(s_1) \frac{\mathbf{Q}_1^4}{(\mathcal{Q}_1^0)^2} F_0^{(2)}(M_{\pi^0}, M_\pi, M_{\pi^0}, M_\pi; s_1) \\
& + 2G''(s_1^+) C_{00}(\tilde{s}_1^{+0}) [C_{+0}(s_1) + E_{+0}^+(s_1, s_2, s_3)] F_0(M_{\pi^0}, M_{\pi^0}, M_\pi, M_{\pi^0}; s_1) \\
& + 2 \left[(G_1 C_{00}(\tilde{s}_1^{+0}) - 2M_K G''(s_1^+) D_{00}) C_{+0}(s_1) \frac{\mathbf{Q}_1^2}{\mathcal{Q}_1^0} - 2G''(s_1^+) C_{00}(\tilde{s}_1^{+0}) E_{+0}(s_1, s_2, s_3) \right] \\
& \quad \times F_0^{(1)}(M_{\pi^0}, M_{\pi^0}, M_\pi, M_{\pi^0}; s_1) \\
& - 4M_K G_1 D_{00} C_{+0}(s_1) \frac{\mathbf{Q}_1^4}{(\mathcal{Q}_1^0)^2} F_0^{(2)}(M_{\pi^0}, M_{\pi^0}, M_\pi, M_{\pi^0}; s_1) + (s_1 \leftrightarrow s_2) \Big\}, \tag{A.2}
\end{aligned}$$

$$\begin{aligned}
\mathcal{M}_N^B & = 4H'(s_3) C_x(s_3) C_{+-}(s_3) J_{+-}^2(s_3) + G(s_3) C_{00}(s_3)^2 J_{00}^2(s_3) + 2G(s_3) C_x(s_3)^2 J_{00}(s_3) J_{+-}(s_3) \\
& + 2H'(s_3) C_x(s_3) C_{00}(s_3) J_{+-}(s_3) J_{00}(s_3) + \left\{ 4G'(s_1) C_{+0}(s_1)^2 J_{+0}^2(s_1) + (s_1 \leftrightarrow s_2) \right\}, \tag{A.3}
\end{aligned}$$

$$\begin{aligned}
\mathcal{M}_C^A & = 2G''(s_3) C_x(\tilde{s}_3^{++}) C_{++}(s_3) F_-(M_{\pi^0}, M_{\pi^0}, M_\pi, M_\pi; s_3) \\
& + 2[G_1 C_x(\tilde{s}_3^{++}) - 2M_K G''(s_3) D_x] C_{++}(s_3) \frac{\mathbf{Q}_3^2}{\mathcal{Q}_3^0} F_-^{(1)}(M_{\pi^0}, M_{\pi^0}, M_\pi, M_\pi; s_3) \\
& - 4M_K G_1 D_x C_{++}(s_3) \frac{\mathbf{Q}_3^4}{(\mathcal{Q}_3^0)^2} F_-^{(2)}(M_{\pi^0}, M_{\pi^0}, M_\pi, M_\pi; s_3) \\
& + 4H''_{+-}(s_3) C_{+-}(\tilde{s}_3^{++}) C_{++}(s_3) F_-(M_\pi, M_\pi, M_\pi, M_\pi; s_3) \\
& - 4 \left[\frac{1}{2} H_1 C_{+-}(\tilde{s}_3^{++}) + 2M_K H''_{+-}(s_3) D_{+-} \right] C_{++}(s_3) \frac{\mathbf{Q}_3^2}{\mathcal{Q}_3^0} F_-^{(1)}(M_\pi, M_\pi, M_\pi, M_\pi; s_3) \\
& + 4M_K H_1 D_{+-} C_{++}(s_3) \frac{\mathbf{Q}_3^4}{(\mathcal{Q}_3^0)^2} F_-^{(2)}(M_\pi, M_\pi, M_\pi, M_\pi; s_3) \\
& + \left\{ 4H''_{+-}(s_1) C_{+-}(\tilde{s}_1^{+-}) [C_{+-}(s_1) - E_{+-}(s_1, s_2, s_3)] F_+(M_\pi, M_\pi, M_\pi, M_\pi; s_1) \right. \\
& - 4 \left[\left(\frac{1}{2} H_1 C_{+-}(\tilde{s}_1^{+-}) + 2M_K H''_{+-}(s_1) D_{+-} \right) C_{+-}(s_1) \frac{\mathbf{Q}_1^2}{\mathcal{Q}_1^0} \right. \\
& \quad \left. \left. - 2H''_{+-}(s_1) C_{+-}(\tilde{s}_1^{+-}) E_{+-}(s_1, s_2, s_3) \right] F_+^{(1)}(M_\pi, M_\pi, M_\pi, M_\pi; s_1) \right. \\
& + 4M_K H_1 D_{+-} C_{+-}(s_1) \frac{\mathbf{Q}_1^4}{(\mathcal{Q}_1^0)^2} F_+^{(2)}(M_\pi, M_\pi, M_\pi, M_\pi; s_1) \\
& + 2G''(s_1) C_x(\tilde{s}_1^{+-}) [C_{+-}(s_1) - E_{+-}(s_1, s_2, s_3)] F_+(M_{\pi^0}, M_{\pi^0}, M_\pi, M_\pi; s_1) \\
& + 2 \left[(G_1 C_x(\tilde{s}_1^{+-}) - 2M_K G''(s_1) D_x) C_{+-}(s_1) \frac{\mathbf{Q}_1^2}{\mathcal{Q}_1^0} \right.
\end{aligned}$$

$$\begin{aligned}
& + 2G''(s_1)C_x(\tilde{s}_1^+)E_{+-}(s_1, s_2, s_3) \Big] F_+^{(1)}(M_{\pi^0}, M_{\pi^0}, M_{\pi}, M_{\pi}; s_1) \\
& - 4M_K G_1 D_x C_{+-}(s_1) \frac{\mathbf{Q}_1^4}{(Q_1^0)^2} F_+^{(2)}(M_{\pi^0}, M_{\pi^0}, M_{\pi}, M_{\pi}; s_1) \\
& + 2H''(s_1)C_{++}(\tilde{s}_1^+) [C_{+-}(s_1) + E_{+-}(s_1, s_2, s_3)] F_+(M_{\pi}, M_{\pi}, M_{\pi}, M_{\pi}; s_1) \\
& + 2 \left[(H_1 C_{++}(\tilde{s}_1^+) - 2M_K H''(s_1) D_{++}) C_{+-}(s_1) \frac{\mathbf{Q}_1^2}{Q_1^0} \right. \\
& \quad \left. - 2H''(s_1) C_{++}(\tilde{s}_1^+) E_{+-}(s_1, s_2, s_3) \right] F_+^{(1)}(M_{\pi}, M_{\pi}, M_{\pi}, M_{\pi}; s_1) \\
& - 4M_K H_1 D_{++} C_{+-}(s_1) \frac{\mathbf{Q}_1^4}{(Q_1^0)^2} F_+^{(2)}(M_{\pi}, M_{\pi}, M_{\pi}, M_{\pi}; s_1) \\
& + 4G_{+0}'''(s_1) C_{+0}(\tilde{s}_1^{00}) C_x(s_1) F_+(M_{\pi}, M_{\pi^0}, M_{\pi^0}, M_{\pi^0}; s_1) \\
& - 4 \left[\frac{1}{2} G_1 C_{+0}(\tilde{s}_1^{00}) + 2M_K G_{+0}'''(s_1) D_{+0} \right] C_x(s_1) \frac{\mathbf{Q}_1^2}{Q_1^0} F_+^{(1)}(M_{\pi}, M_{\pi^0}, M_{\pi^0}, M_{\pi^0}; s_1) \\
& + 4M_K G_1 D_{+0} C_x(s_1) \frac{\mathbf{Q}_1^4}{(Q_1^0)^2} F_+^{(2)}(M_{\pi}, M_{\pi^0}, M_{\pi^0}, M_{\pi^0}; s_1) + (s_1 \leftrightarrow s_2) \Big\}, \tag{A.4}
\end{aligned}$$

$$\begin{aligned}
\mathcal{M}_C^B &= H(s_3) C_{++}(s_3)^2 J_{++}^2(s_3) + \left\{ 4H'(s_1) C_{+-}(s_1)^2 J_{+-}^2(s_1) + G(s_1) C_x(s_1) C_{00}(s_1) J_{00}^2(s_1) \right. \\
& \quad \left. + 2 \left[H'(s_1) C_x(s_1) + G(s_1) C_{+-}(s_1) \right] C_x(s_1) J_{+-}(s_1) J_{00}(s_1) + (s_1 \leftrightarrow s_2) \right\}. \tag{A.5}
\end{aligned}$$

We have used the following abbreviations:

$$\begin{aligned}
C_n(s_i) &= C_n + D_n(s_i - \bar{s}_n), \quad \tilde{s}_i^{cd} = M_c^2 + M_i^2 - s_i + \frac{M_K}{Q_i^0} (s_i + 2\mathbf{Q}_i^2 - M_c^2 + M_d^2), \\
E_{+-}(s_1, s_2, s_3) &= E_{+-} \frac{s_1(s_3 - s_2)}{2M_K Q_1^0}, \quad E_{+0}(s_1, s_2, s_3) = E_{+0} \left[\frac{s_1(s_3 - s_2 - \Delta_\pi)}{2M_K Q_1^0} + \Delta_\pi \right], \\
E_{+0}^\pm(s_1, s_2, s_3) &= E_{+0} \left[\frac{(s_1 \pm \Delta_\pi)(s_3 - s_2 - \Delta_\pi)}{2M_K Q_1^0} + \Delta_\pi \right], \\
G(s_i) &= G_0 + G_1 (p_i^0 - M_\pi) + G_2 (p_i^0 - M_\pi)^2 + G_3 \frac{\mathbf{Q}_i^2}{3} \left(1 - \frac{4M_\pi^2}{s_i} \right), \\
H(s_i) &= H_0 + H_1 (p_i^0 - M_\pi) + H_2 (p_i^0 - M_\pi)^2 + H_3 \frac{\mathbf{Q}_i^2}{3} \left(1 - \frac{4M_\pi^2}{s_i} \right), \\
G'(s_i) &= G_0 + G_1 \left(\frac{Q_i^0}{2} \left(1 + \frac{\Delta_\pi}{s_i} \right) - M_\pi \right) + G_2 \left[\left(\frac{Q_i^0}{2} \left(1 + \frac{\Delta_\pi}{s_i} \right) - M_\pi \right)^2 + \frac{\mathbf{Q}_i^2}{12s_i^2} \lambda(s_i, M_\pi^2, M_{\pi^0}^2) \right] \\
& \quad + G_3 \left[\left(\frac{Q_i^0}{2} \left(1 - \frac{\Delta_\pi}{s_i} \right) - p_i^0 \right)^2 + \frac{\mathbf{Q}_i^2}{12s_i^2} \lambda(s_i, M_\pi^2, M_{\pi^0}^2) \right], \\
H'(s_i) &= H_0 + H_1 \left(\frac{Q_i^0}{2} - M_\pi \right) + H_2 \left[\left(\frac{Q_i^0}{2} - M_\pi \right)^2 + \frac{\mathbf{Q}_i^2}{12} \left(1 - \frac{4M_\pi^2}{s_i} \right) \right] \\
& \quad + H_3 \left[\left(\frac{Q_i^0}{2} - p_i^0 \right)^2 + \frac{\mathbf{Q}_i^2}{12} \left(1 - \frac{4M_\pi^2}{s_i} \right) \right],
\end{aligned}$$

$$\begin{aligned}
G''(s_i) &= G_0 + G_1 \left(\frac{s_i}{2Q_i^0} - M_\pi \right), & G'''_{ab}(s_i) &= G_0 + G_1 \left(\frac{1}{2}(M_K - M_a - M_b) - \frac{s_i}{4Q_i^0} \right), \\
G''(s_i^+) &= G_0 + G_1 \left(\frac{s_i + \Delta_\pi}{2Q_i^0} - M_\pi \right), & G'''_{ab}(s_i^-) &= G_0 + G_1 \left(\frac{1}{2}(M_K - M_a - M_b) - \frac{s_i - \Delta_\pi}{4Q_i^0} \right), \\
H''(s_i) &= H_0 + H_1 \left(\frac{s_i}{2Q_i^0} - M_\pi \right), & H'''_{ab}(s_i) &= H_0 + H_1 \left(\frac{1}{2}(M_K - M_a - M_b) - \frac{s_i}{4Q_i^0} \right), \\
H'''_{ab}(s_i^+) &= H_0 + H_1 \left(\frac{1}{2}(M_K - M_a - M_b) - \frac{s_i + \Delta_\pi}{4Q_i^0} \right).
\end{aligned} \tag{A.6}$$

We remark that the representations of the ‘‘double bubbles’’ $\mathcal{M}_{N/C}^B$ are even *complete* to $\mathcal{O}(a^2\epsilon^6)$ if the polynomials $C_n(s_i)$ are amended by shape parameter terms $\dots + F_n(s_i - \bar{s}_n)^2$: P-wave contributions only start at $\mathcal{O}(a^2\epsilon^8)$. In contrast, in the ‘‘genuine’’ two-loop graphs $\mathcal{M}_{N/C}^A$, terms $\propto E_n F^{(2)}$ have not been included, although they contribute in principle at $\mathcal{O}(a^2\epsilon^6)$. We remark that the two-loop amplitudes for the $K_L \rightarrow 3\pi$ decay channels at the same accuracy can be retrieved from Ref. [29], where the $\eta \rightarrow 3\pi$ amplitudes are discussed within the same formalism, with the obvious replacements as described in Ref. [23].

$F_i(\dots; s)$, $F_i^{(1)}(\dots; s)$, $F_i^{(2)}(\dots; s)$ stand for the integrals $F(\dots; s)$, $F^{(1)}(\dots; s)$, $F^{(2)}(\dots; s)$, evaluated at $\mathbf{Q}^2 = \lambda(M_K^2, M_\pi^2, s)/4M_K^2$, with $i = \pm, 0$. The first few terms in an expansion in ϵ of the analytic expression for these two-loop functions are displayed in Appendix B.

Appendix B. The loop functions F , $F^{(1)}$, and $F^{(2)}$

The functions $F_i(\dots; s)$, $F_i^{(1)}(\dots; s)$, $F_i^{(2)}(\dots; s)$ introduced in Appendix A are explicitly given by

$$\begin{aligned}
F(M_a, M_b, M_c, M_d, s) &= \mathcal{N} \left[2\nu f_1 + \rho f_0 - \frac{3\mathbf{Q}^2}{10s} (\rho f_1 - 2q_0^2 f_0) \right. \\
&\quad \left. + \mathcal{K}(X_3 f_3 + X_2 f_2 + X_1 f_1 + X_0 f_0) \right] + \mathcal{O}(\epsilon^6), \\
F^{(1)}(M_a, M_b, M_c, M_d, s) &= \frac{\mathcal{N}}{10} (1 + \delta) [(10\nu - \rho) f_1 + (5\rho + 2q_0^2) f_0] + \mathcal{O}(\epsilon^4), \\
F^{(2)}(M_a, M_b, M_c, M_d, s) &= \frac{\mathcal{N}}{2} \left[-\frac{1}{\mathbf{Q}^2} (2\nu^2 f_3 + 3\nu\rho f_2 + (\rho^2 - 2\nu q_0^2) f_1 - \rho q_0^2 f_0) \right. \\
&\quad \left. + \frac{(1 + \delta)^2}{4} (\nu f_3 + (\rho - 2\nu) f_2 + (4\nu - 2\rho - q_0^2) f_1 + 2(\rho + q_0^2) f_0) \right] + \mathcal{O}(\epsilon^4),
\end{aligned} \tag{B.1}$$

with

$$\begin{aligned}
\mathcal{N} &= \frac{1}{256\pi^3 \sqrt{s}} \frac{\lambda^{1/2}(s_0, M_a^2, M_b^2)}{s_0 \sqrt{\Delta^2 - \frac{(1+\delta)^2}{4} \mathbf{Q}^2}}, \\
\mathcal{K} &= \left[\frac{1}{2(M_K^2 + M_c^2) - (M_a + M_b)^2 - s_0} + \frac{1}{s_0 - (M_a - M_b)^2} - \frac{2}{s_0} \right] \frac{M_K^2}{s_0 - M_K^2 - M_c^2}, \\
f_0 &= 4(\nu_1 + \nu_2 - \bar{\nu}_2 + h), \quad f_1 = \frac{4}{3} (\nu_1(\nu_1 - 1) + \nu_2(\nu_2 - 1) - \bar{\nu}_2(\bar{\nu}_2 - 1) + h),
\end{aligned}$$

$$\begin{aligned}
f_2 &= -\frac{1}{5\nu}(3\rho f_1 - q_0^2 f_0), \quad f_3 = \frac{1}{7\nu^2}[3(\nu q_0^2 + \rho^2)f_1 - \rho q_0^2 f_0], \\
h &= \frac{1}{2} \ln\left(\frac{1 + \mathbf{Q}^2/s}{1 + \bar{\mathbf{Q}}^2/s_t}\right), \quad \mathbf{Q}^2 = \frac{\lambda(M_K^2, q_3^2, s)}{4M_K^2}, \quad \bar{\mathbf{Q}}^2 = \mathbf{Q}^2(s_t), \quad s_t = (M_c + M_d)^2, \\
v_i &= \sqrt{-y_i} \arctan \frac{1}{\sqrt{-y_i}}, \quad i = 1, 2; \quad \bar{v}_2 = \sqrt{-\bar{y}_2} \arctan \frac{1}{\sqrt{-\bar{y}_2}}, \quad y_{1,2} = \frac{-\rho \mp \sqrt{D}}{2\nu}, \\
\bar{y}_2 &= y_2(s_t), \quad v = -\frac{\mathbf{Q}^2}{s}(M_c^2 + \Delta^2), \quad \rho = q_0^2 - \Delta^2 + \frac{\mathbf{Q}^2}{s}M_c^2, \quad D = \rho^2 + 4\nu q_0^2, \\
X_0 &= (R - H\rho)q_0^2, \quad X_1 = H(\rho^2 - 2\nu q_0^2) - R(2\rho + q_0^2), \quad X_2 = 3H\nu\rho - 3R\left(\nu - \frac{\rho}{2}\right), \\
X_3 &= 2\nu(H\nu + R), \quad H = -\frac{3}{2}\left(1 + \frac{\mathbf{Q}^2}{3s}\right), \quad R = \frac{\mathbf{Q}^2 Q_0^2}{2s}(1 + \delta)^2, \\
s_0 &= M_K^2 + M_c^2 - 2M_K\left(M_c^2 + \frac{\mathbf{Q}^2(1 + \delta)^2}{4}\right)^{1/2}, \quad q_0^2 = \frac{\lambda(s, M_c^2, M_d^2)}{4s}, \\
\Delta^2 &= \frac{\lambda(M_K^2, M_c^2, (M_a + M_b)^2)}{4M_K^2}, \quad \delta = \frac{M_c^2 - M_d^2}{s}, \tag{B.2}
\end{aligned}$$

compare also Fig. 3A. The arctan is understood to be evaluated according to

$$\arctan x = \frac{1}{2i} \ln \frac{1 + ix}{1 - ix}, \tag{B.3}$$

and s is given a small positive imaginary part in all arguments, $s \rightarrow s + i\epsilon$.

Appendix C. Holomorphic properties of F

The loop functions F , $F^{(1)}$, and $F^{(2)}$ in Appendix A are generated by the two-loop graphs displayed in Fig. 3A. The explicit expressions in Appendix B are valid on the upper rim of the real s -axis. Here, we show how to analytically continue them to the whole non-relativistic region. The holomorphic properties of these loop functions play a role in connection with the decomposition of the amplitude as proposed by Cabibbo and Isidori [21], see also the discussion in Appendix H.

The region of holomorphicity could be established directly from the explicit lowest-order expressions given in Appendix B – higher-order terms in ϵ emerge from the Taylor expansion of low-energy polynomials and do not change the analytic structure. Here, we follow a different path and derive the singularity structure from the integral representation Eq. (6.23). To ease notation, we set in this section

$$F(s) \doteq F(M_a, M_b, M_c, M_d; s). \tag{C.1}$$

Appendix C.1. Holomorphic properties from the integral representation

First we note that the prefactor $\mathcal{F}(y, s)$ and the function $g(y, s)$ in the integral representation Eq. (6.23) are low-energy polynomials in $(s - (M_c + M_d)^2)$ and in y . Because the argument of the logarithm does not vanish for $0 \leq y \leq 1$ when s approaches the real axis from above at $\text{Re } s > s_t$, $F(s)$ is analytic in the part of the non-relativistic region located in the upper half of the complex s -plane. To analyze the singularities that may occur during the continuation to the lower rim of

the real axis, we note that $g(y, s)$ has two zeros in the low-energy region, which we denote by $y_1(s)$ and $y_2(s)$,

$$g(y, s) = \frac{\nu}{1 + \frac{\nu Q^2}{s}} (y - y_1(s))(y - y_2(s)), \quad (\text{C.2})$$

where $y_{1,2}(s)$ and ν are defined in Eq. (B.2) [the sign convention is chosen so that $y_1(s) = 0$ at $s = s_t = (M_c + M_d)^2$]. During the analytic continuation, singularities may occur at the following values \bar{s} of s .

- i) $y_{1,2}(\bar{s}) = 0$ or 1. This may generate endpoint singularities.
- ii) If the integration contour runs between $y_1(s)$ and $y_2(s)$, a pinch singularity may occur whenever $y_1(\bar{s}) = y_2(\bar{s})$.
- iii) If $|\lim_{s \rightarrow \bar{s}} y_1(s)| \rightarrow \infty$ or $|\lim_{s \rightarrow \bar{s}} y_2(s)| \rightarrow \infty$, dragging the contour along, the integral in Eq. (6.23) may diverge at \bar{s} and lead to a singularity in $F(s)$.

We now discuss these possibilities in turn.

Appendix C.1.1. Endpoint singularity

The quantity $y_1(s)$ [$y_2(s)$] vanishes linearly [tends to a constant] as $s \rightarrow s_t$, as a result of which the derivative $dF(s)/ds$ diverges at threshold. We conclude that $F(s)$ is singular at $s = s_t$. The case $y_i(\bar{s}) = 1$ does not occur in the low-energy region.

Appendix C.1.2. Pinch singularity

Concerning point ii), we note that $D(\bar{s}) = 0$ is a necessary and sufficient condition for the equality $y_1(\bar{s}) = y_2(\bar{s})$ to hold, see Eq. (B.2). The quantity $D(s)$ may be factorized in the following manner,

$$D(s) = \frac{P(s, q_3^2, M_K^2; M_a, M_b, M_c, M_d) P_L(s, q_3^2, M_K^2; M_a, M_b, M_c, M_d)}{64 M_K^2 M_d^2 s^2}. \quad (\text{C.3})$$

Here, P and P_L denote two polynomials of second order in s . Whereas P has no roots in the low-energy region, the roots of P_L , explicitly given by

$$\begin{aligned} P_L &= \lambda(s, M_d^2, M_c^2) \lambda(q_3^2, (M_a + M_b)^2, M_d^2) - Q^2(s, q_3^2, M_K^2; M_a, M_b, M_c, M_d), \\ Q &= 2M_d^2(M_K^2 - s - q_3^2) + (q_3^2 - (M_a + M_b)^2 + M_d^2)(s + M_d^2 - M_c^2), \end{aligned} \quad (\text{C.4})$$

denote the positions of the potential leading Landau singularities of the relativistic two-loop graph, obtained from Fig. 3A by replacing all propagators with the relativistic ones [57]. We refer the interested reader to Appendix F for a discussion of this point. We conclude that the positions of the potential pinch singularities in the non-relativistic graph Fig. 3A are identical to the location of the leading Landau singularities of the corresponding relativistic Feynman diagram.

The relevant roots of the equation $D(s) = 0$ can be classified according to the values of the masses M_a, M_b, M_c, M_d , and $M_3 = (q_3^2)^{1/2}$. To simplify the discussion, we consider the following three cases, visualized in Fig. 6A–C, see also Fig. 3.

1. Fig. 6A:

The equal-mass case with $M_a = M_b = M_c = M_d = M_3 = M_\pi$. Here, $D(s)$ has a second-order zero on the real axis, at $s = s_1 = (M_K^2 - M_\pi^2)/2$.

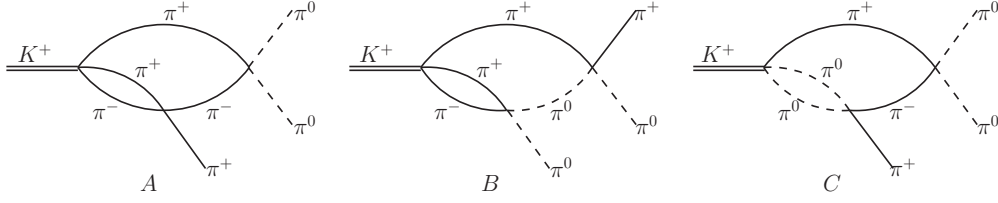


Figure 6: Two-loop graphs contributing to $K^+ \rightarrow \pi^+\pi^0\pi^0$. Their holomorphic properties are discussed in Appendix C (Appendix D and Appendix E) in the case where the propagators are the non-relativistic (the relativistic) ones.

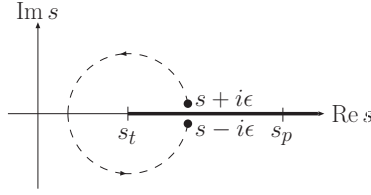


Figure 7: The path in the complex s -plane from the upper rim of the cut to the lower rim. The physical function at real values of s coincides with the boundary value of the analytic function $F(s)$ on the upper rim.

2. Fig. 6B:

$M_a = M_b = M_c = M_\pi$, $M_d = M_3 = M_{\pi^0}$. Here, $D(s)$ has two real roots s_{1-} and s_{1+} ,

$$s_{1\pm} = \frac{1}{2} \left[M_K^2 + 2M_{\pi^0}^2 - 3M_\pi^2 \right] \pm \frac{1}{2M_\pi} \left[(M_\pi^2 - M_{\pi^0}^2) \lambda(M_K^2, M_\pi^2, 4M_{\pi^0}^2) \right]^{1/2}. \quad (\text{C.5})$$

3. Fig. 6C:

$M_a = M_b = M_{\pi^0}$, $M_c = M_d = M_3 = M_\pi$. Here, $D(s)$ has complex-conjugated roots at $s = s_a$, s_a^* in the complex s -plane, with

$$s_a = \frac{1}{2} \left[M_K^2 + 3M_\pi^2 - 4M_{\pi^0}^2 \right] - \frac{i}{2M_{\pi^0}} \left[(M_\pi^2 - M_{\pi^0}^2) \lambda(M_K^2, M_\pi^2, 4M_{\pi^0}^2) \right]^{1/2}. \quad (\text{C.6})$$

Note that the roots differ from each other by terms of $\mathcal{O}(\epsilon^2)$.

Let us now continue $F(s)$ to the lower rim of the real axis, along a generic path near threshold, displayed in Fig. 7. It represents a circle with center at $s = s_t$ and a radius $|s - s_t|$. We assume that $|s - s_t|/(4M_\pi^2)$ is small, such that the zeros of $D(s)$ are avoided. The variable s travels along this circle from the upper rim of the positive real s -axis to its lower rim.

The roots $y_1(s)$ and $y_2(s)$ then move in the complex plane along the trajectories shown in Fig. 8. When $\arg(s - s_t)$ becomes equal to π , the root $y_1(s)$ hits the original integration contour and enforces its deformation. When s approaches the real axis from below, the deformed path looks as follows (see Fig. 8): it starts at $y = 0$, goes in the negative direction, encircles the singularity at $y = y_{\min}(s) = y_1(s)$ and goes back to $y = 1$. To illustrate what happens when a zero of D is encountered, we consider $M_a = M_b = M_{\pi^0}$, $M_c = M_d = M_3 = M_\pi$ (case 3 above), and envisage analytic continuation of $F(s)$ from s_a^* to s_a along the segment of a circle with radius $|s_t - s_a|$. The trajectories of $y_{1,2}(s)$ for the variable s moving along this segment are shown in Fig. 9. Since $y_1(s_a^*) = y_2(s_a^*)$ (and equally for $s_a^* \rightarrow s_a$), the trajectories start at the same point and converge to the same point – the potential generation of a pinch singularity at $s = s_a$ is

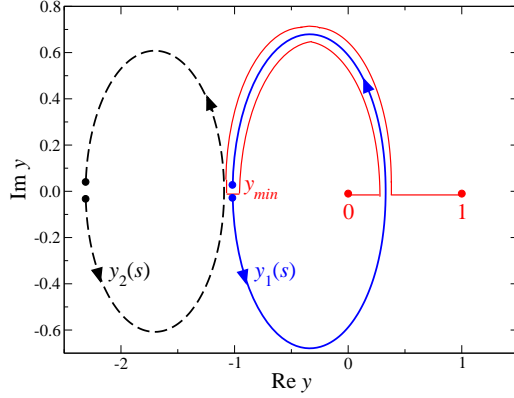


Figure 8: The trajectories of $y = y_1(s)$ and $y = y_2(s)$ in the complex y -plane, when the variable s travels around the generic circle shown in Fig. 7. For $\text{Im } s < 0$ the integration contour has to be deformed as shown, in order to circumvent the singularity at $y = y_1(s)$.

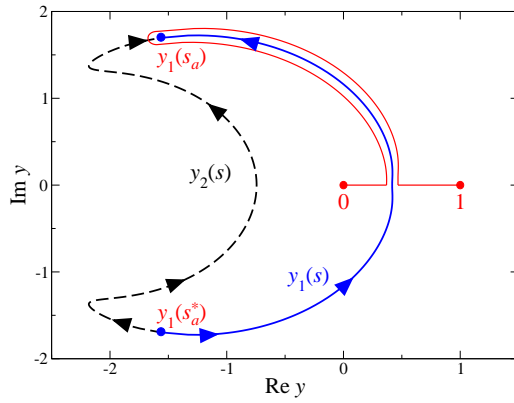


Figure 9: The deformation of the integration contour in the variable y , as s approaches the anomalous threshold s_a .

clearly visible. The cases 1 and 2 look similar. In order to investigate whether these anomalous thresholds really do generate singularities in $F(s)$, we consider the function $H(s)$ defined by

$$H(s) \doteq \int_0^1 \frac{dy}{\sqrt{y}} \left[\frac{d}{dy} \bar{g}(y, s) \right] \ln \bar{g}(y, s), \quad \bar{g}(y, s) = (y - y_1)(y - y_2), \quad (\text{C.7})$$

cf. the integral representation of $F(s)$ in Eq. (6.23). $H(s)$ differs from $F(s)$ only by terms which are irrelevant as far as holomorphic properties are concerned, but is much simpler to discuss. We denote by $H_+(H_-)$ the function $H(s)$, evaluated at the upper (lower) rim of the real s -axis, by continuation according to Fig. 7. We perform a partial integration and obtain

$$H_-(s) = H_+(s) + \frac{4\pi}{3} \sqrt{-y_1} [y_1 + 3y_2], \quad s > s_t. \quad (\text{C.8})$$

Inserting the expressions Eq. (B.2) for $y_{1,2}$, it is seen that the second term on the right hand side

Table 1: The positions of the leading Landau singularities generated by the graphs displayed in Fig. 10 (in MeV).⁵ The quantities $s_a, s_{1\pm}$ denote zeros of the polynomial P_L displayed in Eq. (C.4). For the mass configuration in Fig. 10A (Fig. 10D), $s_a (s_{1\pm})$ is given in Eq. (C.6) (Eq. (C.5)).

| | $\sqrt{s_{1-}}$ | $\sqrt{s_{1+}}$ | $\sqrt{s_a}$ |
|----------|-----------------|-----------------|-----------------|
| <i>A</i> | | | $339.6 - i25.4$ |
| <i>B</i> | | | $339.6 - i25.4$ |
| <i>C</i> | | | $341.6 - i26.7$ |
| <i>D</i> | 308.4 | 355.8 | |
| <i>E</i> | 308.9 | 359.0 | |
| <i>F</i> | 308.9 | 359.0 | |

behaves as follows in the vicinity of the anomalous thresholds,

$$\sqrt{-y_1} [y_1 + 3y_2] = c_0 + \sum_{n=2}^{\infty} c_n (P_L)^{n/2}, \quad c_k \in \mathbb{C}. \quad (\text{C.9})$$

The polynomial P_L is displayed in Eq. (C.4). In other words, the function H_- generates a singularity of the square root type at $s = s_{1\pm}$ ($s = s_a$) in the case 2 (case 3) listed above, whereas it is regular in case 1. The power of the leading singular behavior $\propto (P_L)^{3/2}$ in Eq. (C.9) agrees with the general analysis of these singularities provided in Ref. [38].

It turns out that the topologies displayed in Fig. 6 are the generic ones for the occurrence of leading Landau singularities, in the following sense. At two loops, these singularities occur iff the four-pion vertex at the inner loop amounts to a charge-exchange one, as is the case in Figs. 6B, C. In Fig. 10 we display all two-loop graphs that generate leading Landau singularities, for both $K^+ \rightarrow 3\pi$ and $K_L \rightarrow 3\pi$ decays. The solid (dashed) lines denote charged (neutral) pions, and the double lines incoming kaons. The graphs in Fig. 10A–C (D–E) generate singularities in the complex plane, at $s = s_a$ (on the real axis, at $s = s_{1\pm}$), see Table 1 for numerical values. We conclude that, at two-loop order, leading Landau singularities do occur in *all* decay channels.

The results Eqs. (C.8), (C.9) have important consequences for the decomposition of the amplitudes into regular and singular parts, as proposed in Ref. [21], see Appendix H.

Appendix C.1.3. Singularity at the pseudothreshold

Finally, we discuss singularities at the pseudothreshold $s = s_p \doteq (M_K - M_3)^2$. As can be seen from the explicit expression in Eq. (B.2), $\lim_{s \rightarrow s_p} y_1(s) = -\infty$, whereas y_2 stays finite. From Eq. (C.8), we conclude that H_- therefore tends to infinity as $s \rightarrow s_p - i\epsilon$. The same is therefore true for $F(s)$.

In summary, we conclude that, in the cases 1 and 2, the function $F(s)$ is analytic in the low-energy region of the complex s -plane, cut along the positive axis. The cut starts at the normal threshold $s = s_t = (M_c + M_d)^2$ and extends beyond the pseudothreshold. In the case 3, the cut must be deformed in order to encompass the anomalous threshold at $s = s_a$. We refer the reader to Appendix D and Appendix E for more detailed discussions concerning the relativistic diagrams. The physical values of $F(s)$ are obtained by approaching the real axis from above.

⁵We use the following masses: $M_\pi = 139.6$ MeV, $M_{\pi^0} = 135.0$ MeV, $M_K = M_{K^+} = 493.7$ MeV, $M_{K^0} = 497.6$ MeV.

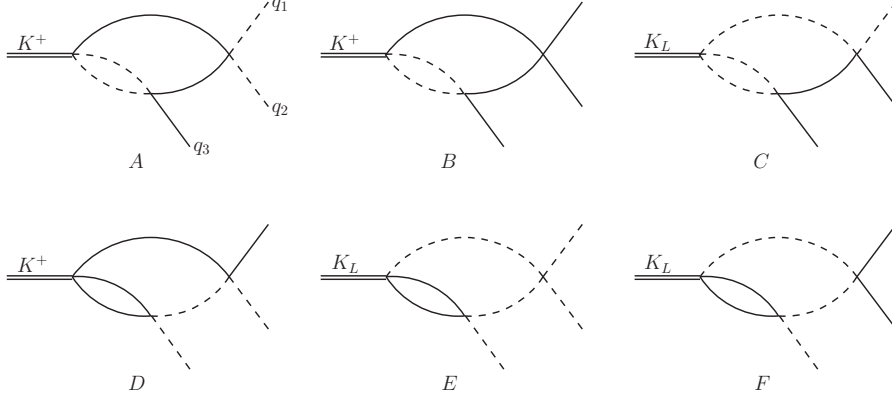


Figure 10: The graphs that generate leading Landau singularities in $K \rightarrow 3\pi$ decays at two-loop order. In Figs. A–C (D–F) the singularities are located in the complex plane, at $s = s_a$ (on the real axis, at $s = s_{1\pm}$), where s denotes the invariant mass of the outgoing two rescattered pions, e.g. $s = (q_1 + q_2)^2$ in graph A. See Table 1 for numerical values.

Appendix C.2. The discontinuity of F

The origin of the discontinuity $\Delta F(s) = F(s + i\epsilon) - F(s - i\epsilon)$ of the function $F(s)$ across the cut was identified above, in case of the function $H(s)$: the integration contours for s located on the upper and on the lower rims of the cut are not the same. In principle, in the same manner, $\Delta F(s)$ could be evaluated from the integral representation Eq. (6.23). For actual calculations this procedure is not very convenient, because $\mathcal{F}(y, s)$ is only known in form of the series Eq. (6.24). For this reason, we now evaluate $\Delta F(s)$ by using a different method.

Since $F(s)$ and $\bar{M}(s)$ only differ by a constant, see Eq. (6.15), we calculate the discontinuity of $\bar{M}(s)$ in the vicinity of the elastic threshold $s = s_t$ and then analytically continue it in s . The discontinuity of $\bar{M}(s)$ in the vicinity of threshold $q_0^2 \ll \Delta^2$ can be obtained directly from Eq. (6.17), since only the first denominator is singular:

$$\begin{aligned} \Delta \bar{M}(s) &= \frac{\pi i}{\sqrt{s}} \int \frac{d^d l}{(2\pi)^d} \frac{d^d k}{(2\pi)^d} \delta(\mathbf{k}^2 - q_0^2) \frac{N(x)}{(\mathbf{l}^2 + \frac{(1+\delta)^2}{4} \mathbf{Q}^2 + x - \Delta^2)} \\ &= -\frac{i q_0}{32\pi^2 \sqrt{s}} \int_{-1}^1 dy N(\hat{x}) \left(\frac{(1+\delta)^2}{4} \mathbf{Q}^2 + \hat{x} - \Delta^2 \right)^{1/2} + \mathcal{O}(d-3), \quad (\text{C.10}) \\ \hat{x} &= q_0^2 + y^2 \frac{q_0^2 \mathbf{Q}^2}{s} + y \frac{q_0 |\mathbf{Q}| \mathcal{Q}^0 (1+\delta)}{\sqrt{s}}, \quad \frac{(1+\delta)^2}{4} \mathbf{Q}^2 + \hat{x} = \left(\frac{\mathcal{Q}^0 (1+\delta)}{2} + y \frac{q_0 |\mathbf{Q}|}{\sqrt{s}} \right)^2 - M_c^2. \end{aligned}$$

Calculating the integral over y , we obtain

$$\Delta \bar{M}(s) = -\frac{1}{128\pi^2 \sqrt{s}} (\Phi(q_0) - \Phi(-q_0)), \quad (\text{C.11})$$

where

$$\begin{aligned} \Phi(y) &= a \ln \left(\sqrt{b - c_- a - y} + \sqrt{b - c_+ a - y} \right) - \sqrt{(b - c_- a - y)(b - c_+ a - y)} \\ &\quad + 2a \sqrt{c_+ c_-} \ln \frac{\sqrt{c_+(b - c_- a - y)} + \sqrt{c_-(b - c_+ a - y)}}{\sqrt{b - y}}, \quad (\text{C.12}) \end{aligned}$$

and

$$a = \frac{2(M_a^2 + M_b^2)\sqrt{s}}{2M_K|\mathbf{Q}|}, \quad b = \frac{(M_K^2 + M_c^2 - M_K Q_0(1 + \delta))\sqrt{s}}{2M_K|\mathbf{Q}|}, \quad c_{\pm} = \frac{(M_a \pm M_b)^2}{2(M_a^2 + M_b^2)}. \quad (\text{C.13})$$

Closer inspection of the trajectory of $y_1(s)$, see Fig. 8, shows that, in order to perform the analytic continuation consistently, the variable s in the discontinuity should have an infinitesimal *negative* imaginary part, $s \rightarrow s - i\epsilon$.

Appendix D. Relativistic two-loop integrals – equal pion masses

The evaluation of the two-loop graphs Fig. 3A in the non-relativistic theory is presented in Sect. 6, and the holomorphic properties of the pertinent loop functions are discussed in Appendix C. The procedure is quite complex and non-standard. We therefore wish to compare the result with the calculation in relativistic quantum field theory, where the propagators in Fig. 3A are taken to be the relativistic ones. In this and the following Appendix, we discuss this more standard calculation, and, in particular, the holomorphic properties of the pertinent loop functions. We stick here to the three topologies shown in Fig. 6. In Appendix D (Appendix E), we consider the case of equal (unequal) pion masses running in the loops, see Fig. 6A (Figs. 6B, C). We use scalar vertices throughout, because derivative couplings do not change the holomorphic properties of the integrals. A comparison between the two approaches is provided in Appendix G, where we show that the non-relativistic calculation approximates the relativistic one in a well-defined manner – as it must be for the present framework to make sense.

Appendix D.1. Notation

We use dimensional regularization and put

$$\omega = \frac{D}{2} - 2, \quad (\text{D.1})$$

where D denotes the dimension of space-time. Loop integrations are symbolized by a bracket,

$$\langle \dots \rangle_l = \int \frac{d^D l}{i(2\pi)^D} (\dots), \quad \langle \langle \dots \rangle \rangle_{lk} = \int \frac{d^D l}{i(2\pi)^D} \int \frac{d^D k}{i(2\pi)^D} (\dots). \quad (\text{D.2})$$

We abbreviate Feynman parameter integrals by

$$\{ \dots \}_1 = \int_0^1 dx_1 \{ \dots \}, \quad \{ \dots \}_{12} = 2 \int_0^1 dx_1 \int_0^1 x_2 dx_2 \{ \dots \}. \quad (\text{D.3})$$

Furthermore, we use the measure

$$[d\sigma] = \frac{C(\omega)\Gamma(3/2)}{\Gamma(3/2 + \omega)} \frac{\sigma^\omega}{4^\omega} \left(1 - \frac{4M_\pi^2}{\sigma} \right)^{\omega+1/2} d\sigma, \quad (\text{D.4})$$

with

$$C(\omega) = \frac{1}{(4\pi)^{2+\omega}}. \quad (\text{D.5})$$

Further, in order to simplify the notation, we will suppress the dependence of the various loop functions on the meson masses.

Appendix D.2. The loop function $\bar{K}(s)$

As mentioned, we first consider the case where the masses of all pions running in the loops, as well as of the outgoing pion with momentum q_3 , are taken to be equal [cf. Figs. 3A and 6A],

$$M_a = M_b = M_c = M_d = M_\pi, \quad q_3^2 = M_\pi^2. \quad (\text{D.6})$$

The fact that we consider two neutral pions in one of the vertices does not change the holomorphic properties of the graph, as these pions enter the final expression only through the square of their total four momentum, $s = (q_1 + q_2)^2$. The pertinent loop integral is

$$G(s) = \left\langle \left\langle \frac{1}{D_1 D_2 D_3 D_4} \right\rangle \right\rangle_{lk}, \quad (\text{D.7})$$

with

$$D_1 = M_\pi^2 - k^2, \quad D_2 = M_\pi^2 - (Q - k)^2, \quad D_3 = M_\pi^2 - l^2, \quad D_4 = M_\pi^2 - (P_K - l - k)^2, \quad (\text{D.8})$$

and

$$Q^\mu = (P_K - q_3)^\mu, \quad P_K^2 = M_K^2, \quad Q^2 = s. \quad (\text{D.9})$$

The integral $G(s)$ is proportional to the quantity V_{121} investigated in great detail for real external momenta in Ref. [57]. In particular, these authors have set up codes to evaluate the ultraviolet finite part of $G(s)$ by numerical integration. Here, the purpose is quite different: we wish to investigate the holomorphic properties of $G(s)$ as well. Our method to evaluate these integrals is therefore necessarily very different from the one developed in Ref. [57].

We proceed in two steps. First, we identify the part of $G(s)$ that stays finite as $D \rightarrow 4$ by subtracting the divergent subintegral and by removing the remaining overall divergence. In the second step, we express the finite part through a once subtracted dispersion relation in the variable s .

To start with, we consider the inner loop

$$J(t) = \left\langle \frac{1}{D_3 D_4} \right\rangle_l = C(\omega) \Gamma(-\omega) \{z^\omega\}_1, \quad z = M_\pi^2 - x_1(1 - x_1)t, \quad t = (P_K - k)^2. \quad (\text{D.10})$$

It is useful to write $J(t)$ in a dispersive manner [58],

$$J(t) = \int_{4M_\pi^2}^{\infty} \frac{[d\sigma]}{\sigma - t}, \quad (\text{D.11})$$

and to single out its divergence at $D = 4$,

$$J(t) = J(0) + \bar{J}(t),$$

such that $G(s)$ in Eq. (D.7) becomes

$$G(s) = J(s)J(0) + K(s), \quad K(s) = \int_{4M_\pi^2}^{\infty} \frac{[d\sigma]}{\sigma} \left\langle \frac{t}{D_1 D_2 (\sigma - t)} \right\rangle_k. \quad (\text{D.12})$$

This integral has still an overall divergence at $D = 4$. It can be made finite by subtracting its value at $s = 0$,

$$K(s) = K(0) + \bar{K}(s). \quad (\text{D.13})$$

As a result, one has

$$G(s) = J(s)J(0) + K(0) + \bar{K}(s). \quad (\text{D.14})$$

We now discuss the finite part $\bar{K}(s)$.

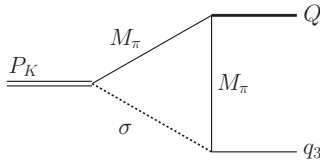


Figure 11: The triangle graph which corresponds to the amplitude $T(s)$ in Eq. (D.15). We use $P_K^\mu = (Q + q_3)^\mu$, $Q^2 = s$, $q_3^2 = M_\pi^2$, $P_K^2 = M_K^2$.

Appendix D.3. Peculiarities of $\bar{K}(s)$

To illustrate the difficulties one is faced with when investigating the holomorphic properties of $\bar{K}(s)$, we first consider the one-loop integral $J(t)$ in Eq. (D.10), in D dimensions. The $i\epsilon$ prescription for the square of the masses in the propagators is equivalent to providing the variable t with a positive imaginary part: the integral Eq. (D.10) defines a function $\mathcal{J}(t)$ which is holomorphic in the upper half plane $\text{Im } t > 0$, and real on the real axis for $t < 4M_\pi^2$. It may therefore be holomorphically continued to the lower half plane through the Schwarz reflection principle. The denominator z vanishes at two points $x_{1,2} \in (0, 1)$ for $t > 4M_\pi^2$. Therefore, $\mathcal{J}(t)$ is holomorphic in the complex plane, cut along the real axis for $\text{Re } t \geq 4M_\pi^2$, and $J(t)$ is the boundary value $J(t) = \lim_{\text{Im } t \rightarrow 0^+} \mathcal{J}(t)$. The dispersive representation in Eq. (D.11) is based on these observations.

This chain of arguments cannot be carried over to $\bar{K}(s)$ without further ado. To show why this is so, we consider the integrand

$$T(s) = \left\langle \frac{1}{D_1 D_2 (\sigma - t)} \right\rangle_k, \quad \sigma \geq 4M_\pi^2, \quad t = (P_K - k)^2 \quad (\text{D.15})$$

in Eq. (D.12) [we drop t in the numerator, because this does not affect the analytic properties of $T(s)$]. The quantity $T(s)$ corresponds to the triangle diagram displayed in Fig. 11.

The integral is ultraviolet convergent and can thus be evaluated at $D = 4$. After integration over the momentum k , we are left with the Feynman parameter integral

$$T(s) = \{z^{-1}\}_{12}, \quad z = x_2^2 M_\pi^2 + \sigma(1 - x_2) - x_2 x_1 \{s(1 - x_1)x_2 + (1 - x_2)(M_K^2 - M_\pi^2)\} - i\epsilon. \quad (\text{D.16})$$

We have explicitly displayed the $i\epsilon$ prescription. In this case, we cannot replace $i\epsilon$ by providing s with a positive imaginary part: the denominator z vanishes at two points on the $x_1 = 1$ boundary, for any value of s , provided that $M_K > \sqrt{\sigma} + M_\pi$, a condition which is met for the physical value of the kaon mass. In other words, at $\epsilon = 0$, the integral Eq. (D.16) is not well defined for real, physical values of M_π^2, M_K^2 , at any s , and cannot straightforwardly be considered to be the boundary value of a holomorphic function $\mathcal{T}(s)$. This renders the discussion more complicated than in the case of $J(s)$ [59]. A similar remark applies to $\bar{K}(s)$.

A way out of the problem is based on the following observation. First, examining Eq. (D.16), one notes that $T(s)$ has a unique extension $\mathcal{T}(s)$ into the product of the upper half complex planes of s and M_K^2 .⁶ One then considers the kaon mass to be an adjustable parameter [45, 59, 60]. For

⁶It was already noted in Ref. [39] that $T(s)$ is holomorphic when all three variables M_K^2 , s , and q_3^2 lie in the same half planes.

sufficiently small value of M_K^2 , the above-mentioned problem does not exist – the function $\mathcal{T}(s)$ satisfies an unsubtracted dispersion relation in the variable s , with threshold $s_t = 4M_\pi^2$. For physical values of the kaon mass, $\mathcal{T}(s)$ is then defined by analytic continuation of the dispersive representation through the upper complex M_K^2 -plane, and $T(s) = \lim_{\text{Im } s \rightarrow 0^+, \text{Im } M_K \rightarrow 0^+} \mathcal{T}(s)$ [45, 59, 60].

This procedure may now be directly carried over to $\bar{K}(s)$ – the final integration over σ in Eq. (D.12) does not affect the arguments just outlined, aside from the necessity to use a subtracted dispersion relation. Concerning the continuation in M_K^2 , we consider the Cauchy representation

$$\bar{K}(s) = \frac{s}{2\pi i} \int_{4M_\pi^2}^C \frac{dx \Delta \bar{K}(x)}{x(x-s)}, \quad (\text{D.17})$$

where C denotes the path of integration in the complex s -plane, and $\Delta \bar{K}$ stands for the discontinuity of \bar{K} across C . For small kaon masses, C may be taken to run along the real axis from $4M_\pi^2$ to infinity, and \bar{K} is holomorphic in the complex s -plane, cut along C . The discontinuity is itself a holomorphic function $\Delta \bar{K}(s)$ in a certain region of the complex s -plane, with singularities $s_i(M_K, M_\pi)$ whose positions depend on the pion and kaon masses. These singularities generate singularities in the function \bar{K} on higher Riemann sheets. During the process of increasing the value of the kaon mass to its physical mass, one has to make sure that the singularities s_i do not cross the path C , by eventually deforming it properly [45, 59, 60] – in other words, the singularities in \bar{K} may eventually move to the first Riemann sheet. Once the continuation has been accomplished, it is straightforward to read off the analytic properties of $\bar{K}(s)$, together with e.g. its threshold behavior, which is of particular interest in our case. Finally, one has $\bar{K}(s) = \lim_{\text{Im } s \rightarrow 0^+, \text{Im } M_K \rightarrow 0^+} \bar{K}(s)$.

Appendix D.4. The discontinuity $\Delta \bar{K}$

It remains to evaluate the discontinuity in the dispersive representation Eq. (D.17). For sufficiently small values of the kaon mass, unitarity of the S -matrix fixes it unambiguously. It is given by the angular integral⁷

$$\begin{aligned} \Delta \bar{K}(s) &= \frac{iv(s)}{256\pi^3} \int_{-1}^1 dz \left\{ \beta(z) \ln \frac{\beta(z)-1}{\beta(z)+1} + 2 \right\}, \quad s \in [4M_\pi^2, \infty]; \quad v(s) = \left(1 - \frac{4M_\pi^2}{s} \right)^{1/2}, \\ \beta(z) &= \left(1 - \frac{4M_\pi^2}{A+Bz} \right)^{1/2}, \quad A = \frac{1}{2} [M_K^2 + 3M_\pi^2 - s], \quad B = \frac{v(s)}{2} \lambda^{1/2}(s, M_K^2, M_\pi^2). \end{aligned} \quad (\text{D.18})$$

After the substitution $(\beta(z)-1)/(\beta(z)+1) = u$, the integral can straightforwardly be performed. For the following discussions, it is useful to introduce the functions

$$\begin{aligned} \Phi(x, y; z_+, z_-; m) &= m^2(r_+^2 - r_-^2) - (x+y)z_+r_+ + (x-y)z_-r_-, \quad r_\pm = \ln(1+z_\pm) - \ln(z_\pm - 1), \\ F(x, y; z_+, z_-; m) &= \Phi(x, y; z_+, z_-; m)|_{r_\pm \rightarrow R_\pm}, \quad R_\pm = \ln(1+z_\pm) - \ln(1-z_\pm), \\ G(x, y; z_+, z_-; m) &= 2m^2(R_- + R_+) - (x+y)z_+ - (x-y)z_-. \end{aligned} \quad (\text{D.19})$$

⁷Here and below, we denote the independent variable in the discontinuity with s .

The discontinuity for small values of the kaon mass is given by

$$\Delta\bar{\mathcal{K}}(s) = \frac{i\nu(s)}{256\pi^3} \left[6 + B^{-1}D(s) \right], \quad D(s) = \Phi(A, B; W_+, W_-; M_\pi), \quad W_\pm = \left(1 - \frac{4M_\pi^2}{A \pm B} \right)^{1/2}. \quad (\text{D.20})$$

According to the discussion above, this representation must be continued analytically to the physical value of M_K^2 . Potential singularities in the discontinuity occur for those values of s where the arguments of W_\pm vanish, or B vanishes. To investigate the first possibility, we observe that the quantity $(A - 4M_\pi^2)^2 - B^2$ agrees up to a factor with the polynomial P_{6A} in Eq. (F.3) that determines the location of potential leading Landau singularities in the graph Fig. 6A,

$$(A - 4M_\pi^2)^2 - B^2 = \frac{4M_\pi^2}{s} (s - s_1)^2, \quad s_1 = \frac{1}{2}(M_K^2 - M_\pi^2). \quad (\text{D.21})$$

The zeros of B occur at $s = 4M_\pi^2, (M_K \pm M_\pi)^2$. Because M_K^2 is equipped with a positive imaginary part, the zeros at $s = s_1, (M_K \pm M_\pi)^2$ are located above the path C of integration. At $s = 4M_\pi^2$, the discontinuity vanishes.

There are thus four intervals to be distinguished,

| | | | | | |
|----------|--------------|--------------|--------------|-----------------|--------|
| Interval | IIIb | IIIa | II | I | |
| | $[s_t, s_1]$ | $[s_1, s_p]$ | $[s_p, s_c]$ | $[s_c, \infty)$ | (D.22) |

where

$$s_t = 4M_\pi^2, \quad s_p = (M_K - M_\pi)^2, \quad s_c = (M_K + M_\pi)^2. \quad (\text{D.23})$$

We now list the discontinuity in the four intervals for physical values of the kaon mass, and use the notation

$$\bar{B} = \frac{\nu(s)}{2} |\lambda(s, M_K^2, M_\pi^2)|^{1/2}. \quad (\text{D.24})$$

Interval I [$\Delta\bar{\mathcal{K}}$ is imaginary]

Here, $B = \bar{B}$, and $W_\pm - 1 > 0$. The discontinuity may therefore simply be evaluated from the expression given in Eq. (D.20). As a check we have verified that the expression for $\Delta\bar{\mathcal{K}}$, evaluated at $M_K = M_\pi = 1$, agrees with the discontinuity of the two-loop function \bar{V}_1 worked out in Ref. [58, Appendix A.2].

Interval II [$\Delta\bar{\mathcal{K}}$ is imaginary]

The function $D(s)$ is evaluated as in interval I, with $B = -i\bar{B}$.

Interval III [$\Delta\bar{\mathcal{K}}$ is complex]

In this interval, $B = -\bar{B}$, and the discontinuity is obtained from

$$D(s) = i\pi G(A, B; W_+, W_-; M_\pi) + F(A, B; W_+, W_-; M_\pi), \quad W_\pm = c_\pm \left| 1 - \frac{4M_\pi^2}{A \pm B} \right|^{1/2}. \quad (\text{D.25})$$

The numbers c_\pm are

| | | | |
|----------|------|------|--------|
| Interval | IIIa | IIIb | |
| c_+ | 1 | -1 | (D.26) |
| c_- | 1 | 1 | |

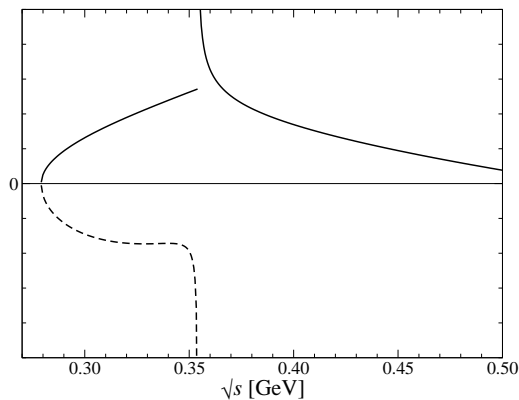


Figure 12: The discontinuity $\Delta\bar{\mathcal{K}}(s)$ as a function of \sqrt{s} , in the equal mass case, in arbitrary units. The solid (dashed) curve stands for the imaginary (real) part of $\Delta\bar{\mathcal{K}}$. The singularity at the pseudothreshold $\sqrt{s_p}$ is clearly seen.

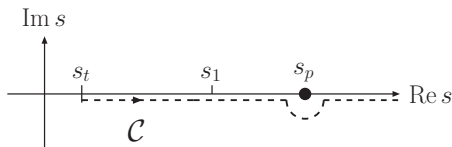


Figure 13: The path C in the dispersive integral Eq. (D.17), for physical kaon mass. The symbols s_t , s_1 , and s_p are defined in Eq. (D.23).

The discontinuity develops a singularity at the pseudothreshold $s = s_p$. This is due to the fact that the angular integral in Eq. (D.18) must be deformed to infinity in the complex plane as s approaches s_p [45], and the angular integral finally diverges at $s = s_p$. On the other hand, there is no singularity at $s = s_1$ [second order zero in Eq. (D.21)].

In Fig. 12, we display the discontinuity $\Delta\bar{\mathcal{K}}(s)$ as a function of \sqrt{s} . The solid (dashed) curve stands for the imaginary (real) part of $\Delta\bar{\mathcal{K}}$. The singularity at the pseudothreshold s_p is clearly visible. From the explicit expression of the discontinuity, one furthermore concludes that it generates a square root singularity at threshold,

$$\Delta\bar{\mathcal{K}}(s) = v(s)d(s), \quad (\text{D.27})$$

with $d(s)$ holomorphic at $s = 4M_\pi^2$.

Appendix D.5. Holomorphic properties of $\bar{\mathcal{K}}(s)$

We deform the path C in the representation Eq. (D.17) such that the singularity of the discontinuity at the pseudothreshold s_p is avoided in the manner indicated in Fig. 13, as is requested by the continuation in M_K^2 . The function $\bar{\mathcal{K}}(s)$ is thus holomorphic in the complex s -plane, cut along the real axis for $s \geq 4M_\pi^2$. Furthermore, on the upper rim of the cut, it is holomorphic as well. The singularity of the discontinuity at $s = s_p$ shows up in $\bar{\mathcal{K}}(s)$ only on the lower rim of the cut, where it diverges when s_p is approached from below. We may perform the dispersion integral Eq. (D.17) numerically. The result is displayed in Fig. 14, with the variable s at the upper rim of the cut.

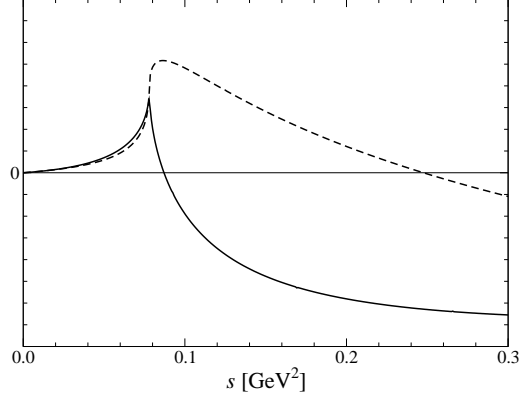


Figure 14: The function $\tilde{\mathcal{K}}(s)$ evaluated numerically from Eq. (D.17), in arbitrary units, with s at the upper rim of the cut. The solid (dashed) line denotes the real (imaginary) part of $\tilde{\mathcal{K}}(s)$.

Appendix E. Relativistic two-loop integrals – unequal pion masses

We now investigate the graphs Fig. 6B, C, see also Fig. 3A. The corresponding ultraviolet finite loop functions $\tilde{\mathcal{K}}_{B,C}$ are again written as a dispersive integral,

$$\tilde{\mathcal{K}}_I(s) = \frac{s}{2\pi i} \int_{(M_c+M_d)^2}^{\infty} \frac{dx \Delta \tilde{\mathcal{K}}_I(x)}{x(x-s)}, \quad I = B, C. \quad (\text{E.1})$$

The discontinuities are given by angular integrals

$$\Delta \tilde{\mathcal{K}}_I(s) = \frac{iv_{cd}(s)}{256\pi^3} \int_{-1}^1 \left\{ \beta_I(z) \ln \frac{\beta_I(z) - 1}{\beta_I(z) + 1} + 2 \right\} dz; \quad s \in [(M_c + M_d)^2, \infty],$$

where

$$v_{cd}(s) = \frac{\lambda^{1/2}(s, M_c^2, M_d^2)}{s}, \quad \beta_B(z) = \left(1 - \frac{M_\pi^2}{\hat{A} + \hat{B}z} \right)^{1/2}, \quad \beta_C(z) = \left(1 - \frac{M_{\pi^0}^2}{\hat{A} + \hat{B}z} \right)^{1/2},$$

$$\hat{A} = M_K^2 + M_c^2 - \frac{1}{2s}(s + M_c^2 - M_d^2)(M_K^2 + s - q_3^2), \quad \hat{B} = \frac{v_{cd}(s)}{2} \lambda^{1/2}(s, M_K^2, q_3^2). \quad (\text{E.2})$$

For later use, we introduce

$$\tilde{B} = \frac{v_{cd}(s)}{2s} |\lambda(s, M_K^2, q_3^2)|^{1/2}. \quad (\text{E.3})$$

Appendix E.1. Case I

We first consider the graph in Fig. 6B,

$$M_a = M_b = M_c = M_\pi, \quad M_d = M_{\pi^0}, \quad q_3^2 = M_{\pi^0}^2. \quad (\text{E.4})$$

Singularities are generated by the zeros in

$$\hat{W}_\pm = \left(1 - \frac{4M_\pi^2}{\hat{A} \pm \hat{B}} \right)^{1/2}. \quad (\text{E.5})$$

The quantity $(\hat{A} - 4M_\pi^2)^2 - \hat{B}^2$ agrees up to a factor with the polynomial P_{6B} in Eq. (F.3), which shows that corresponding singularities in $\Delta\bar{\mathcal{K}}_B$ occur at

$$s_{1\pm} = \frac{1}{2} \left[M_K^2 + 2M_{\pi^0}^2 - 3M_\pi^2 \right] \pm \frac{1}{2M_\pi} \left[(M_\pi^2 - M_{\pi^0}^2) \lambda(M_K^2, M_\pi^2, 4M_\pi^2) \right]^{1/2}. \quad (\text{E.6})$$

We have to distinguish the following intervals:

$$\begin{array}{cccccc} \text{Interval} & \text{IIIc} & \text{IIIb} & \text{IIIa} & \text{II} & \text{I} \\ & [s_t, s_{1-}] & [s_{1-}, s_{1+}] & [s_{1+}, s_p] & [s_p, s_c] & [s_c, \infty) \end{array} \quad (\text{E.7})$$

where

$$s_t = (M_{\pi^0} + M_\pi)^2, \quad s_p = (M_K - M_{\pi^0})^2, \quad s_c = (M_K + M_{\pi^0})^2. \quad (\text{E.8})$$

The discontinuity is

$$\Delta\bar{\mathcal{K}}_B = \frac{iv_{+0}(s)}{256\pi^3} \left[6 + \hat{B}^{-1} \hat{D}_B(s) \right], \quad (\text{E.9})$$

where $\hat{D}_B(s)$ is given by the following expressions in the intervals I–III:

Interval I [$\Delta\bar{\mathcal{K}}_B$ is imaginary]

Here, one has $\hat{B} = \bar{B}$, and

$$\hat{D}_B(s) = \Phi(\hat{A}, \hat{B}; W_+, W_-; M_\pi), \quad W_\pm = \left(1 - \frac{4M_\pi^2}{\hat{A} \pm \hat{B}} \right)^{1/2}. \quad (\text{E.10})$$

Interval II [$\Delta\bar{\mathcal{K}}_B$ is imaginary]

The discontinuity is evaluated as in interval I, with $\hat{B} = -i\bar{B}$.

Interval III [$\Delta\bar{\mathcal{K}}_B$ is complex]

In this interval, one uses $\hat{B} = -\bar{B}$, and

$$\hat{D}_B(s) = i\pi G(\hat{A}, \hat{B}; W_+, W_-; M_\pi) + F(\hat{A}, \hat{B}; W_+, W_-; M_\pi), \quad W_\pm = c_\pm \left| 1 - \frac{4M_\pi^2}{\hat{A} \pm \hat{B}} \right|^{1/2}, \quad (\text{E.11})$$

where

$$\begin{array}{cccc} \text{Interval} & \text{IIIa} & \text{IIIb} & \text{IIIc} \\ c_+ & 1 & -i & -1 \\ c_- & 1 & 1 & 1 \end{array} \quad (\text{E.12})$$

Appendix E.2. Holomorphic properties of $\bar{\mathcal{K}}_B$

The discontinuity $\Delta\bar{\mathcal{K}}_B$ develops a singularity of the square root type at $s = s_{1\pm}$. The path of integration in the dispersive representation Eq. (E.1) is indicated in Fig. 15. The function $\bar{\mathcal{K}}_B$ is holomorphic in the complex s -plane, cut along the positive real axis for $s \geq (M_{\pi^0} + M_\pi)^2$. It is as well holomorphic at the upper rim of the cut, and diverges at the pseudothreshold $s = s_p$ when approached from below the cut. Further, at $s = s_{1\pm}$, it has singularities of the square root type on the lower rim of the cut. Its precise behavior there is indicated in Eq. (C.9).

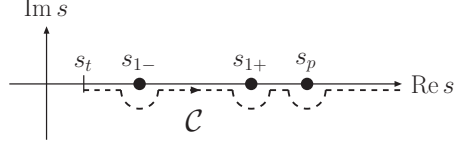


Figure 15: The path C in the dispersive integral Eq. (E.1), with mass assignments as displayed in Eq. (E.4), for physical kaon mass. The symbols s_t , s_{1-} , s_{1+} , and s_p denote threshold, two anomalous thresholds, and the pseudothreshold, respectively, and are given explicitly in Eqs. (E.6), (E.8).

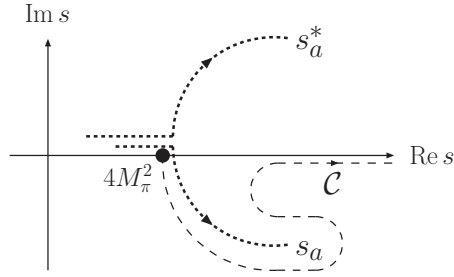


Figure 16: The singularities s_a, s_a^* in the discontinuity $\Delta\tilde{\mathcal{K}}_C(s)$, for the mass assignments Eq. (E.13), as a function of the kaon mass (dotted lines). The symbol s_a is defined in Eq. (F.4), s_a^* denotes its complex conjugate, and the arrows indicate the direction of increasing kaon masses. The singularity s_a intrudes into the original path of integration, such that C must be deformed [dashed line], see also Fig. 17.

Appendix E.3. Case II

Finally, we consider the case where the pions in the inner loop are neutral and all the others charged,

$$M_a = M_b = M_{\pi^0}, \quad M_c = M_d = M_{\pi}, \quad q_3^2 = M_{\pi}^2, \quad (\text{E.13})$$

see Figs. 3A, 6C. This case is the most intriguing one. Performing the angular integral in Eq. (E.2) and investigating the singularities as before, we find that the ones in the pertinent square roots \hat{W}_{\pm} are given by the polynomial P_{6C} displayed in Eq. (F.3). We display the locations of the singularities s_a, s_a^* as a function of the kaon mass in Fig. 16 [dotted lines]. We see that, as the kaon mass is increased, the singularity $s = s_a$ intrudes into the original path of integration. As a result, the path C must be modified [dashed line], see also Fig. 17.

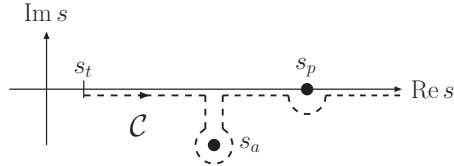


Figure 17: The path C in the dispersive integral Eq. (E.1), with mass assignments as displayed in Eq. (E.13), for physical kaon mass. The symbols s_t , s_a , and s_p are defined in Eqs. (D.23) and (F.4).

Appendix E.4. Holomorphic properties of $\bar{\mathcal{K}}_C$

From the above discussion, we conclude that $\bar{\mathcal{K}}_C(s)$ is holomorphic in the complex s -plane, cut along the path C displayed in Fig. 17. It is holomorphic at the upper rim of the cut, and diverges at the pseudothreshold s_p when approached from below. Further, at $s = s_a$, it develops a singularity of the square root type on the lower rim of the cut. Its precise behavior there is the one indicated in Eq. (C.9). The singularity at s_a^* is located on the second Riemann sheet.

Appendix F. Leading Landau singularities

Some of the graphs that correspond to Fig. 3A have the property that they generate singularities that correspond to the solutions of the pertinent leading-order Landau equations. These singularities occur because the kaon is unstable. The positions of these singularities are given by the two solutions of a polynomial equation of second order in s [57],

$$P_L(s, q_3^2, M_K^2; M_a, M_b, M_c, M_d) = 0, \quad (\text{F.1})$$

with

$$\begin{aligned} P_L &= \lambda(s, M_d^2, M_c^2) \lambda(q_3^2, (M_a + M_b)^2, M_d^2) - Q^2(s, q_3^2, M_K^2; M_a, M_b, M_c, M_d), \\ Q &= 2M_d^2(M_K^2 - s - q_3^2) + (q_3^2 - (M_a + M_b)^2 + M_d^2)(s + M_d^2 - M_c^2). \end{aligned} \quad (\text{F.2})$$

For the graphs Figs.6A–C, this polynomial becomes

$$\begin{aligned} P_{6A} &= P_L(s, M_\pi^2, M_K^2; M_\pi, M_\pi, M_\pi, M_\pi) = -16M_\pi^4 [s - s_1]^2, \\ P_{6B} &= P_L(s, M_{\pi^0}^2, M_K^2; M_\pi, M_\pi, M_\pi, M_{\pi^0}) = -16M_\pi^2 M_{\pi^0}^2 [s - s_{1+}] [s - s_{1-}], \\ P_{6C} &= P_L(s, M_\pi^2, M_K^2; M_{\pi^0}, M_{\pi^0}, M_\pi, M_\pi) = -16M_\pi^2 M_{\pi^0}^2 [s - s_a] [s - s_a^*]. \end{aligned} \quad (\text{F.3})$$

Here, s_a^* denotes the complex conjugate of s_a . The thresholds are

$$\begin{aligned} s_1 &= \frac{1}{2}(M_K^2 - M_\pi^2), \\ s_{1\pm} &= \frac{1}{2} \left[M_K^2 + 2M_{\pi^0}^2 - 3M_\pi^2 \right] \pm \frac{1}{2M_\pi} \left[(M_\pi^2 - M_{\pi^0}^2) \lambda(M_K^2, M_\pi^2, 4M_\pi^2) \right]^{1/2}, \\ s_a &= \frac{1}{2} \left[M_K^2 + 3M_\pi^2 - 4M_{\pi^0}^2 \right] - \frac{i}{2M_{\pi^0}} \left[(M_\pi^2 - M_{\pi^0}^2) \lambda(M_K^2, M_\pi^2, 4M_{\pi^0}^2) \right]^{1/2}. \end{aligned} \quad (\text{F.4})$$

The positions of the leading Landau singularities of the triangle graph displayed in Fig. 18 are obtained from a polynomial equation $P_T(s, q_3^2, M_K^2; M_X, M_c, M_d) = 0$ [37]. It is interesting to note that, for $M_X = M_a + M_b$, the polynomials P_L and P_T are proportional to each other, and the positions of the leading Landau singularities in the two-loop graphs Fig. 3A and the triangle graph Fig. 18 thus coincide. This corroborates the statement made in Ref. [59, Section 3] on the origin of the singularities in the graph 6A.

The discussions in the previous appendices show that the discontinuities of the graphs in Fig. 6B, C do have a singularity at $s_{1\pm}$, s_a , s_a^* , while the one of Fig. 6A is holomorphic at s_1 . As a result of this, the pertinent loop functions generate square root singularities at $s_{1\pm}$, s_a on the lower rim of the cut.

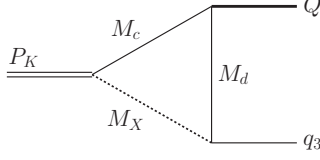


Figure 18: The triangle graph with general masses. The positions of its leading Landau singularities agree with those of the two-loop graphs in Fig. 3A for $M_X = M_a + M_b$, for general q_3^2 . The notation is $P_K^\mu = (Q + q_3)^\mu$, $Q^2 = s$, $P_K^2 = M_K^2$.

Appendix G. Relativistic vs. non-relativistic approach

As already mentioned in Appendix D, the non-relativistic calculations should reproduce the relativistic results graph by graph in a systematic expansion in ϵ – otherwise, the whole framework does not make sense. In other words, it should be possible to adjust the couplings in the non-relativistic Lagrangian at order ϵ^n so that the relativistic expression of any graph, expanded in powers of ϵ , up to and including $\mathcal{O}(\epsilon^n)$ would be reproduced by a uniquely identifiable set of non-relativistic graphs.

In this Appendix, we check this equivalence for the relativistic two-loop graph, considered in Appendix D. To this end, we first compare the expression for the non-relativistic discontinuity, Eq. (C.11), to the expression obtained in the relativistic theory. For simplicity, we restrict ourselves to the case $M_a = M_b = M_c = M_d = M_3 = M_\pi$. The comparison is carried out in the threshold region IIIb defined in Eq. (D.22) where the non-relativistic expression has been originally derived. The discontinuity in the whole non-relativistic region is obtained by using analytic continuation.

The quantities A and \bar{B} , which were defined in the relativistic theory, see Eqs. (D.18) and (D.24), are related to the quantities a , b , q_0 through

$$a = \frac{4M_\pi^2}{\kappa}, \quad b = \frac{A}{\kappa}, \quad q_0 = \frac{\bar{B}}{\kappa}, \quad \kappa = \frac{2M_K|\mathbf{Q}|}{\sqrt{s}}. \quad (\text{G.1})$$

From the above equation we find (cf. Eq. (D.20))

$$\left(1 - \frac{a}{b \pm q_0}\right)^{1/2} = \left(1 - \frac{4M_\pi^2}{A \pm \bar{B}}\right)^{1/2} = \bar{W}_\pm \quad (\text{G.2})$$

and

$$\begin{aligned} \Phi(q_0) - \Phi(-q_0) &= \frac{\sqrt{s}}{2M_K|\mathbf{Q}|} \left(2M_\pi^2(\bar{R}_- - \bar{R}_+) + (A + \bar{B})\bar{W}_+ - (A - \bar{B})\bar{W}_-\right), \\ \bar{R}_\pm &= \ln(1 + \bar{W}_\pm) - \ln(1 - \bar{W}_\pm). \end{aligned} \quad (\text{G.3})$$

The final expression for the non-relativistic discontinuity is obtained by substituting Eq. (G.3) into Eq. (C.11). It is seen that this expression differs from the pertinent relativistic expression given by Eqs. (D.20), (D.24), (D.25) by

$$\text{Disc}_s(s)|_{Rel} - \text{Disc}_s(s)|_{NR} = 2iv(s)P(s), \quad P(s) = \frac{1}{512\pi^3} \left(6 - \frac{F}{\bar{B}}\right), \quad (\text{G.4})$$

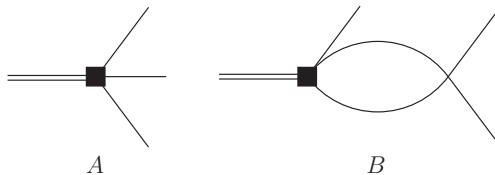


Figure 19: Non-relativistic diagrams that remove the right-hand side of Eq. (G.4). The thick squares stand for the counterterms in the non-relativistic $K \rightarrow 3\pi$ Lagrangian at order a .

where $v(s) = (1 - 4M_\pi^2/s)^{1/2}$, and F is defined in Eq. (D.19). One may ensure that the quantity $P(s)$ is a low-energy polynomial with real coefficients. Consequently, the relativistic and non-relativistic amplitudes themselves differ by $iv(s)P(s) + P'(s)$, where $P'(s)$ is another low-energy polynomial.

In order to establish the origin of the above polynomials, let us first compare the relativistic and non-relativistic one-loop integrals in the vicinity of the threshold. As seen from Eq. (2.9), only the imaginary part of the one-loop integral above threshold survives in the non-relativistic approach (the expression below threshold is obtained through analytic continuation). This corresponds to the following replacement in the expression of the one-loop integral $\bar{J}(s)$ above threshold

$$v(s) \ln \frac{v(s) - 1}{v(s) + 1} + 2 = v(s) \ln \frac{1 - v(s)}{1 + v(s)} + 2 + i\pi v(s) \rightarrow i\pi v(s). \quad (\text{G.5})$$

The dropped part is a low-energy polynomial with real coefficients (in the whole non-relativistic region) and corresponds to adding the counterterms to the $K \rightarrow 3\pi$ vertex shown in Fig. 19A. The numerical values of these counterterms are fixed at order a .

It can be straightforwardly checked that inserting the vertices with the counterterms inside the pion loop, as shown in Fig. 19B, and evaluating this diagram in the non-relativistic theory yields exactly the result $iv(s)P(s)$. Consequently, this term takes into account the renormalization in the non-relativistic theory at $O(a)$. Finally, the polynomial $P'(s)$ corresponds to the renormalization of the $K \rightarrow 3\pi$ vertices at $O(a^2)$. At the order we are working, only tree diagrams with these counterterms contribute.

To summarize, we have demonstrated that all differences between the relativistic and non-relativistic amplitudes in the low-energy region can be removed by changing the renormalization prescription in the $K \rightarrow 3\pi$ vertices. Consequently, relativistic and non-relativistic theories are physically equivalent at this order. Obviously, this also holds for the expansion of the pertinent Feynman graphs in powers of ϵ .

Appendix H. The decomposition $\mathcal{M} = \mathcal{M}_0 + v_{cd}\mathcal{M}_1$

One of the crucial ingredients in the work of Cabibbo and Isidori [21] is the decomposition of the decay amplitudes \mathcal{M} into the form

$$\mathcal{M} = \mathcal{M}_0 + v_{cd}(s)\mathcal{M}_1. \quad (\text{H.1})$$

The amplitudes $\mathcal{M}_{0,1}$ are assumed to be analytic in the physical region of the decays, with square root singularities at the border of the Dalitz plot, associated with different $\pi\pi$ thresholds [2].

In this Appendix, we comment on this decomposition, and start the discussion with a simpler case, the relativistic one-loop integral

$$J_{cd}(s) = \left\langle \frac{1}{M_c^2 - l^2} \frac{1}{M_d^2 - (l - P)^2} \right\rangle_l, \quad s = P^2. \quad (\text{H.2})$$

Let

$$\bar{J}_{cd}(s) = J_{cd}(s) - J_{cd}(0). \quad (\text{H.3})$$

The function \bar{J}_{cd} is analytic in the complex s -plane, cut along the real axis for $s \geq (M_c + M_d)^2$. Its explicit form near the threshold $s = (M_c + M_d)^2$ is indeed of the form Eq. (H.1). Define \mathcal{M}_0 through

$$\bar{J}_{cd}(s) = \mathcal{M}_0 + \frac{i v_{cd}(s)}{16\pi}. \quad (\text{H.4})$$

It then follows that \mathcal{M}_0 has no right hand cut, because the term $i v_{cd}(s)/16\pi$ reproduces the discontinuity of $\bar{J}(s)$ at $s > (M_c + M_d)^2$. On the other hand, this term develops singularities at the pseudothreshold $s = (M_c - M_d)^2$, and at $s = 0$. Because \bar{J}_{cd} is analytic there, the amplitude \mathcal{M}_0 develops the same singularities, with opposite sign, such that the sum is regular at these points. Since $s = 0, s = (M_c - M_d)^2$ are outside the kinematic region of interest in the present case, these singularities do not matter, and one concludes that $\bar{J}_{cd}(s)$ indeed has a decomposition Eq. (H.1) with amplitudes $\mathcal{M}_{0,1}$ that enjoy the properties proposed in Ref. [2].

For the two-loop graphs discussed above, the situation is more complex. Let us first discuss the situation in case of the function $H(s)$ introduced in Eq. (C.8), with mass assignments that correspond to the diagram Fig. 6B. We start from the discontinuity

$$\Delta H(s) \doteq H_+(s) - H_-(s) = -\frac{4\pi}{3} \sqrt{-y_1} (y_1 + 3y_2), \quad s > (M_\pi + M_{\pi^0})^2, \quad (\text{H.5})$$

worked out in Eq. (C.8). We note that $y_1 = -v_{+0}^2 f_1(v_{+0}^2), y_2 = -f_2(v_{+0}^2)$ near threshold, with $f_i(z)$ holomorphic at $z = 0$, and $f_i(0) > 0$. Now define the amplitude $H_0(s)$ through

$$H(s) = \frac{1}{2} \Delta H(s) + H_0(s), \quad s > (M_{\pi^0} + M_\pi)^2. \quad (\text{H.6})$$

Evaluating the discontinuity on both sides, it is seen that H_0 is holomorphic near threshold. Therefore,

$$H(s) = H_0(s) + v_{+0} H_1(s), \quad H_1 = \frac{1}{2v_{+0}} \Delta H(s), \quad (\text{H.7})$$

with $H_{0,1}$ holomorphic at threshold. However, as is shown in Appendix C.1.2, ΔH is singular at $s = s_{1\pm}$. Because $H(s)$ is regular there, H_0 must be singular as well. A completely analogous argument may be used to discuss the inadequacy of the decomposition (H.1) in case of the relativistic integral discussed in Appendix E.1. Numerical values for the positions of these singularities are provided in Table 1.

We find it instructive to display the singular behavior of $\mathcal{M}_{0,1}$ in a fully explicit manner, in a simplified example inspired by the relativistic integrals discussed in Appendix E. Consider the dispersive integral

$$I(s) = \frac{1}{\Delta} \int^C \frac{dx \sqrt{x - 4M_\pi^2} \sqrt{s_{1-} - x}}{x - s}, \quad s \notin C. \quad (\text{H.8})$$

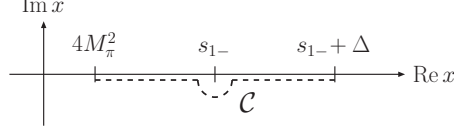


Figure 20: The path C along which the integral is taken in Eq. (H.8).

Here, $\sqrt{x - 4M_\pi^2}$ stands for the standard phase space factor, $\sqrt{s_{1-} - x}$ is a substitute for the square-root singularity in the discontinuity at $s = s_{1-}$, and Δ denotes a (mass-scale)² specified below. The path C is indicated in Fig. 20, compare with Fig. 15.

The function $I(s)$ is holomorphic in the complex s -plane, cut along the real axis for $s \in [4M_\pi^2, s_{1-} + \Delta]$. Further, $I(s)$ can be holomorphically continued through the upper rim of the cut, because the singularity at $s = s_{1-}$ is not effective there – the path C can be suitably deformed. On the other hand, approaching the cut from below, it is seen that C cannot be deformed any more at $s = s_{1-}$, as a result of which one encounters a (pinch) singularity there.

To perform the integration, we set $\Delta = s_{1-} - 4M_\pi^2$, $x = 4M_\pi^2 + \Delta y$,

$$I(s) = G(z) \doteq \lim_{\epsilon \rightarrow 0^+} \int_0^2 \frac{dy \sqrt{y} \sqrt{1-y+i\epsilon}}{y-z}, \quad z = \frac{s - 4M_\pi^2}{\Delta}. \quad (\text{H.9})$$

We find

$$G(z) = \int_0^1 \frac{dy \sqrt{y} \sqrt{1-y}}{y-z} + i \int_1^2 \frac{dy \sqrt{y} \sqrt{y-1}}{y-z} = G_1(z) + iG_2(z), \quad (\text{H.10})$$

with

$$\begin{aligned} G_1 &= i\pi \sqrt{z} \sqrt{1-z} + p_1(z), & G_2 &= \sqrt{z} \sqrt{1-z} \arctan \frac{4\sqrt{z} \sqrt{1-z}}{(3z-2)\sqrt{2}} + p_2(z), \\ p_1 &= -\pi \left(z - \frac{1}{2} \right), & p_2 &= \sqrt{2} + \ln \left(3 + 2\sqrt{2} \right) \left(z - \frac{1}{2} \right), \end{aligned} \quad (\text{H.11})$$

where z is located on the upper rim of the cut, near $z = 0$. One concludes that

$$I(s) = i \sqrt{s - 4M_\pi^2} I_1(s) + I_0(s), \quad I_1 = \frac{\pi}{\Delta} \sqrt{s_{1-} - s}, \quad I_0 = p_1(z) + iG_2(z), \quad (\text{H.12})$$

with $I_{0,1}$ holomorphic at threshold. This is indeed a decomposition of the type Eq. (H.1). Note, however, that I_1 develops a square root singularity at $s = s_{1-}$. As was said above, $I(s)$ is holomorphic on the upper rim of the cut. Therefore, I_0 develops a singularity at $s = s_{1-}$ as well, canceling the one generated by I_1 . Indeed, near $z = 1$, one has

$$G_2 = \sqrt{z} \sqrt{1-z} \left[\arctan \frac{4\sqrt{z} \sqrt{1-z}}{(3z-2)\sqrt{2}} - \pi \right] + p_2(z), \quad (\text{H.13})$$

as a result of which the singularities in $I_{0,1}$ cancel in the sum (H.12). On the other hand, on the lower rim of the cut, near $s = s_{1-}$, the singularities add, and $I(s)$ shows a square root behavior.

References

- [1] P. Budini and L. Fonda, Phys. Rev. Lett. **6** (1961) 419.
- [2] N. Cabibbo, Phys. Rev. Lett. **93** (2004) 121801 [arXiv:hep-ph/0405001].
- [3] J. R. Batley *et al.* [NA48/2 Collaboration], Phys. Lett. B **633** (2006) 173 [arXiv:hep-ex/0511056].
- [4] G. Colangelo, J. Gasser and H. Leutwyler, Phys. Lett. B **488** (2000) 261 [arXiv:hep-ph/0007112].
- [5] G. Colangelo, J. Gasser and H. Leutwyler, Nucl. Phys. B **603** (2001) 125 [arXiv:hep-ph/0103088].
- [6] S. M. Roy, Phys. Lett. B **36** (1971) 353.
- [7] S. Weinberg, Physica A **96** (1979) 327.
- [8] J. Gasser and H. Leutwyler, Annals Phys. **158** (1984) 142.
- [9] J. L. Uretsky and T. R. Palfrey, Phys. Rev. **121** (1961) 1798.
- [10] B. Adeva *et al.*, CERN proposal CERN/SPSLC 95-1, 1995.
- [11] B. Adeva *et al.* [DIRAC Collaboration], Phys. Lett. B **619** (2005) 50 [arXiv:hep-ex/0504044].
- [12] B. Ananthanarayan, G. Colangelo, J. Gasser and H. Leutwyler, Phys. Rept. **353** (2001) 207 [arXiv:hep-ph/0005297].
- [13] S. Descotes-Genon, N. H. Fuchs, L. Girlanda and J. Stern, Eur. Phys. J. C **24** (2002) 469 [arXiv:hep-ph/0112088].
- [14] S. Pislak *et al.*, Phys. Rev. D **67** (2003) 072004 [Erratum-ibid. D **81** (2010) 119903] [arXiv:hep-ex/0301040].
- [15] J. R. Batley *et al.* [NA48/2 Collaboration], Eur. Phys. J. C **54** (2008) 411.
- [16] J. R. Batley *et al.* [NA48/2 Collaboration], Eur. Phys. J. C **70** (2010) 635.
- [17] J. R. Batley *et al.* [NA48/2 Collaboration], Eur. Phys. J. C **64** (2009) 589 [arXiv:0912.2165 [hep-ex]].
- [18] J. Gasser, PoS **KAON** (2008) 033 [arXiv:0710.3048 [hep-ph]].
- [19] G. Colangelo, J. Gasser and A. Rusetsky, Eur. Phys. J. C **59** (2009) 777 [arXiv:0811.0775 [hep-ph]].
- [20] A. Rusetsky, PoS **CD09** (2009) 071 [arXiv:0910.5151 [hep-ph]].
- [21] N. Cabibbo and G. Isidori, JHEP **0503** (2005) 021 [arXiv:hep-ph/0502130].
- [22] G. Colangelo, J. Gasser, B. Kubis and A. Rusetsky, Phys. Lett. B **638** (2006) 187 [arXiv:hep-ph/0604084].
- [23] M. Bissegger, A. Fuhrer, J. Gasser, B. Kubis and A. Rusetsky, Phys. Lett. B **659** (2008) 576 [arXiv:0710.4456 [hep-ph]].
- [24] M. Bissegger, A. Fuhrer, J. Gasser, B. Kubis and A. Rusetsky, Nucl. Phys. B **806** (2009) 178 [arXiv:0807.0515 [hep-ph]].
- [25] W. E. Caswell and G. P. Lepage, Phys. Lett. B **167** (1986) 437.
- [26] J. Gasser, V. E. Lyubovitskij and A. Rusetsky, Phys. Rept. **456** (2008) 167 [arXiv:0711.3522 [hep-ph]].
- [27] B. Kubis, EPJ Web Conf. **3** (2010) 01008 [arXiv:0912.3440 [hep-ph]].
- [28] C.-O. Gullström, A. Kupś and A. Rusetsky, Phys. Rev. C **79** (2009) 028201 [arXiv:0812.2371 [hep-ph]].
- [29] S. P. Schneider, B. Kubis and C. Ditsche, JHEP **1102** (2011) 028 [arXiv:1010.3946 [hep-ph]].
- [30] B. Kubis and S. P. Schneider, Eur. Phys. J. C **62** (2009) 511 [arXiv:0904.1320 [hep-ph]].
- [31] A. Fuhrer, Phys. Lett. B **683** (2010) 172 [arXiv:0909.3121 [hep-ph]].
- [32] A. Fuhrer, Phys. Lett. B **692** (2010) 130 [arXiv:1007.0031 [hep-ph]].
- [33] R. Oehme, Phys. Rev. **111** (1958) 1430.
- [34] R. Karplus, C. M. Sommerfield and E. H. Wichmann, Phys. Rev. **111** (1958) 1187.
- [35] Y. Nambu, Nuovo Cim. **9** (1958) 610.
- [36] L. D. Landau, Nucl. Phys. **13** (1959) 181.
- [37] R. Eden, P. V. Landshoff, D. I. Olive and J. C. Polkinghorne, *The analytic S-matrix*, Cambridge University Press, 1966.
- [38] N. Nakanishi, *Graph theory and Feynman integrals*, Gordon and Breach, 1971.
- [39] G. Källén and A. Wightman, Mat. Fys. Skr. Dan. Vid. Selsk. **1** No. 6 (1958).
- [40] A. Ferroglia, M. Passera, G. Passarino and S. Uccirati, Nucl. Phys. B **650** (2003) 162 [arXiv:hep-ph/0209219].
- [41] M. Beneke and V. A. Smirnov, Nucl. Phys. B **522** (1998) 321 [arXiv:hep-ph/9711391].
- [42] V. Antonelli, A. Gall, J. Gasser and A. Rusetsky, Annals Phys. **286** (2001) 108 [arXiv:hep-ph/0003118].
- [43] M. Knecht and R. Urech, Nucl. Phys. B **519** (1998) 329 [arXiv:hep-ph/9709348].
- [44] E. Braaten and A. Nieto, Phys. Rev. B **55** (1997) 8090 [arXiv:hep-th/9609047].
- [45] V. V. Anisovich and A. A. Ansel'm, Sov. Phys. Uspekhi **9** (1966) 117 [Usp. Fiz. Nauk **88** (1966) 287].
- [46] A. Nehme, Phys. Rev. D **70** (2004) 094025 [arXiv:hep-ph/0406209].
- [47] J. Bijnens and F. Borg, Eur. Phys. J. C **39** (2005) 347 [arXiv:hep-ph/0410333].
- [48] J. Bijnens and F. Borg, Eur. Phys. J. C **40** (2005) 383 [arXiv:hep-ph/0501163].
- [49] E. Gámiz, J. Prades and I. Scimemi, Eur. Phys. J. C **50** (2007) 405 [arXiv:hep-ph/0602023].
- [50] S. R. Gevorkyan, A. V. Tarasov and O. O. Voskresenskaya, Phys. Lett. B **649** (2007) 159 [arXiv:hep-ph/0612129].
- [51] S. R. Gevorkyan, D. T. Madigozhin, A. V. Tarasov and O. O. Voskresenskaya, Phys. Part. Nucl. Lett. **5** (2008) 85 [arXiv:hep-ph/0702154].

- [52] S. R. Gevorkyan, A. V. Tarasov and O. O. Voskresenskaya, *Eur. Phys. J. C* **67** (2010) 143 [arXiv:0910.3904 [hep-ph]].
- [53] G. Isidori, *Eur. Phys. J. C* **53** (2008) 567 [arXiv:0709.2439 [hep-ph]].
- [54] K. Kampf, M. Knecht, J. Novotný and M. Zdráhal, *Nucl. Phys. Proc. Suppl.* **186** (2009) 334 [arXiv:0810.1906 [hep-ph]].
- [55] K. Kampf, M. Knecht, J. Novotný and M. Zdráhal, arXiv:1103.0982 [hep-ph].
- [56] J. R. Batley *et al.* [NA48/2 Collaboration], *Phys. Lett. B* **686** (2010) 101 [arXiv:1004.1005 [hep-ex]].
- [57] A. Ferroglia, M. Passera, G. Passarino and S. Uccirati, *Nucl. Phys. B* **680** (2004) 199 [arXiv:hep-ph/0311186].
- [58] J. Bijnens, G. Colangelo, G. Ecker, J. Gasser and M. E. Sainio, *Nucl. Phys. B* **508** (1997) 263 [Erratum-ibid. **B 517** (1998) 639] [arXiv:hep-ph/9707291].
- [59] G. Barton and C. Kacser, *Nuovo Cim.* **21** (1961) 593.
- [60] C. Fronsdal and R.E. Norton, *J. Math. Phys.* **5** (1963) 100.